



## **School of Chemistry**

Production of black diamond by chemical vapour deposition for testing as an antimicrobial surface.

Tara Zoë May

**This thesis is submitted in partial fulfilment of the requirements for the Honours  
Degree of BSc at the University of Bristol**

Supervisor: Paul May

Second Assessor: Neil Fox

Physical and Theoretical Group

## Abstract

Antibiotic resistance is a growing issue in today's world, making the development of new antimicrobial strategies increasingly important. Antimicrobial surfaces that employ micro or nanostructures to kill bacteria by mechanical rupture of the cell membrane are an important area of research as bacteria are less likely to become resistant to this type of physical bactericidal mechanism. Originally inspired by nature, micro and nanostructured surfaces have been recreated using a range of synthetic materials, including black silicon. Black silicon is an etched form of silicon covered in high aspect ratio nanoprotusions which have been shown to have bactericidal properties against Gram-positive and Gram-negative bacteria. Coating these needles in a thin film of diamond by chemical vapour deposition produces black diamond which reduces the fragility of the needles while maintaining good bactericidal properties.

This work builds on previous studies of black diamond as an antibacterial surface, with the majority of the project focusing on optimising the seeding and growth times of black silicon samples to produce black diamond samples suitable for biological testing. Black silicon samples are seeded with a range of seeding suspensions and grown for different lengths of time in the hot filament reactor to be analysed by SEM. Growth times of 30 minutes were found to be optimal and it was observed that increasing the sonication time of the nanodiamond seeding suspension improved the quality of the diamond film grown.

A set of samples were therefore grown for 30 minutes and produced black diamond samples with needles of  $\sim 3.0 \mu\text{m}$  height,  $\sim 300 \text{ nm}$  tip diameter and  $\sim 8 \mu\text{m}^{-2}$  density. These samples have been sent to Groningen University for bactericidal testing using Gram-positive bacteria *Staphylococcus aureus* and *Staphylococcus epidermidis*.

## **Acknowledgements**

I would like to thank my supervisor Paul May for his help and guidance with my project throughout the year. Also, thanks to Ed Smith for all his extremely valuable help in the lab, for obtaining our many SEM images and for all the general advice he gave me with my project. Additionally, thanks to Gulnur Zulpukarova with whom I really enjoyed working with for all those growth runs and who was also a massive help generally. Additionally, thanks to Neil Fox and the rest of the diamond group for their insights and support.

# Contents

<b>1 Introduction.....</b>	<b>5</b>
1.1 Bacteria and other microorganisms.....	5
1.1.1 Biofilms.....	5
1.1.2 Bacteria .....	5
1.1.3 Viruses .....	5
1.1.4 Algae.....	6
1.2 Antimicrobial surfaces .....	6
1.2.1 Antimicrobial surfaces in nature.....	7
1.2.2 Physical mechanism of cell death on nanostructured surfaces .....	9
1.2.3 Synthetic antibacterial surfaces.....	11
1.3 Black silicon (bSi).....	15
1.4 Black diamond (bD).....	17
1.4.1 Diamond.....	18
1.4.2 Surface Termination.....	20
1.5 Previous Work .....	21
1.6 Project Aims.....	22
<b>2 Methodology .....</b>	<b>23</b>
2.1 Sample preparation .....	23
2.1.1 Black silicon.....	23
2.1.2 Seeding.....	23
2.1.3 Diamond growth .....	23
2.2 Characterisation of samples .....	25
2.2.1 Scanning Electron Microscopy .....	25
2.2.2 Raman Spectroscopy.....	25
2.3 Fragility test .....	25
<b>3 Results and Discussion.....</b>	<b>26</b>
3.1 Optimising seeding and growth time .....	26
3.2 Raman .....	37
3.3 Fragility experiment.....	39
<b>4 Conclusion .....</b>	<b>42</b>
<b>5 Future Work.....</b>	<b>43</b>
<b>7 Appendix.....</b>	<b>47</b>
7.1 Raman .....	47

# 1 Introduction

## 1.1 Bacteria and other microorganisms

Infections caused by bacteria and other microorganisms are a growing problem in our society, especially with the development of antibiotic resistance making existing methods of treating these infections less viable.<sup>1</sup> A newer strategy that deals with the problem of bacterial growth is antimicrobial surfaces: several strategies are used for the design of these surfaces but here we focus on surfaces with a nanotopography that kills cells via a biophysical mechanism.

### 1.1.1 Biofilms

Biofilms form when microorganisms accumulate on a surface or in a separate aggregate. The cells produce extracellular polymeric substances such as proteins, lipids, polysaccharides, and extracellular DNA (eDNA) which form a protective matrix. This matrix is what protects the biofilm from external threats such as antibiotics and makes them such a significant cause of infection.<sup>2</sup> Several types of microorganisms such as bacteria<sup>3</sup>, viruses<sup>4</sup>, fungi<sup>3</sup> and algae<sup>5</sup> are able to form biofilms but have different characteristics and structures which means they have different effects and also require different strategies to manage.

### 1.1.2 Bacteria

Bacteria are single-celled organisms typically  $0.4 - 3.0 \mu\text{m}^3$  in volume<sup>6</sup>; they can be classified as Gram-positive and Gram-negative. This categorisation was developed by Christian Gram in 1884 and relies on the structure of the cell retaining the 'Gram stain' (Gram-positive) or not (Gram-negative). The most significant structural difference between these types of bacteria is in the cell wall. Gram-positive bacteria have a thick peptidoglycan layer but no outer membrane whereas Gram-negative bacteria have only a thin peptidoglycan layer and an outer membrane with a lipopolysaccharide component. Peptidoglycan is responsible for the rigidity and shape of the cell: it consists of repeating units of *N*-acetylglucosamine and *N*-acetyl muramic acid, with peptide side chains cross-linking between them.<sup>7</sup>

### 1.1.3 Viruses

Viruses have also been shown to be capable of forming biofilms.<sup>4</sup> While their size greatly varies between species, viruses are generally smaller than bacteria with a typical size of about 100 nm diameter. They are also structurally very different and cannot survive for long without a host cell in which they can create new virus particles. Therefore, viruses will naturally not survive for as long on surfaces but strategies to decrease this time further is still useful in reducing infection.<sup>8</sup>

### **1.1.4 Algae**

Another microorganism capable of forming biofilms is algae. These microorganisms can exist as single cells or in clusters, with enormous size variation of single cells ranging from 0.5  $\mu\text{m}$  to 50  $\mu\text{m}$  in diameter.<sup>9</sup> While not quite as relevant in terms of human infection, algae biofilms tend to form in marine environments. For example, algae biofilm formation on submerged ship hulls increases the drag of the moving ship and therefore increases fuel consumption.<sup>10</sup>

## **1.2 Antimicrobial surfaces**

Significant research has been done to develop strategies to prevent the formation of biofilms, with one area being antimicrobial surfaces. Antimicrobial surfaces have great potential to be used in healthcare settings, for example in medical implants and surgical instruments<sup>11</sup>, as they have the effect of reducing the attachment and spread of bacteria on a surface, preventing the formation of biofilm which is the source of infection.<sup>12</sup> This is particularly important as biofilms tend to be more resistant to traditional antibiotics once they have formed.<sup>13</sup>

These surfaces can be classified according to how they achieve this: antibiofouling surfaces prevent cells from attaching to the surface whereas bactericidal surfaces kill the cells that come into contact with the surface. Surfaces can be designed to be both antibiofouling and bactericidal.<sup>12</sup>

Previously, a variety of approaches have been employed when designing antimicrobial surfaces, including surface modification and surface coating techniques. Surface coating involves covering the surface in an antibacterial material that either releases an antibacterial reagent or is toxic to bacteria on contact.<sup>14</sup> For example, silver-based coatings are used as they release bactericidal silver ions<sup>15</sup> whereas compounds such as quaternary ammonium compounds (QACs) act by killing bacteria on contact.<sup>16</sup> There are several drawbacks to this method: these coatings often lack long term stability and the issue of developing antibiotic resistance is still present.<sup>12</sup> Another method involves modifying the chemistry of the surface in various ways including by adsorption of antimicrobial agents such as polymers, enzymes and peptides<sup>17</sup> or introducing functional groups which enhance the efficacy of antimicrobial surfaces by covalent linkages, polymerisation or plasma treatment.<sup>12</sup>

Another type of antimicrobial surface involves modifying the surface topography to have a mechanical effect on bacterial cells. This type of surface normally has nanoscale structural features which will damage cells that come into contact with it. The benefit of this type of surface is that mechanical mechanisms of cell death have a reduced risk of the bacteria developing resistance to them compared to chemical methods such as antibiotics.<sup>18</sup>

### 1.2.1 Antimicrobial surfaces in nature

Surfaces with these nanoscale structural features that have antibacterial properties are present in many instances in nature and have inspired the design of a new type of synthetic antibacterial surface. Investigation of both synthetic and natural antibacterial surfaces has allowed the comparison of the efficacy of different characteristics of the nanostructures and the chemistry of the surface.

Examples of antimicrobial surfaces in nature include the wings of insects such as cicada<sup>18</sup>, damselflies<sup>19</sup>, and dragonflies<sup>20</sup> as well as plant leaves<sup>21</sup>, shark skin<sup>22</sup> and gecko skin<sup>23</sup>. These surfaces can prevent biofilms from forming due to superhydrophobicity, self-cleaning ability, bactericidal properties or a combination of these features.<sup>11</sup>

The role of surface nanofeatures on bacteria was first investigated by Ivanova *et al.* when studying bacterial adhesion on the wings of the *Psaltoda claripennis* species of cicada, it was discovered that the wing surface was having a bactericidal effect on the cells studied (*Pseudomonas aeruginosa*) due to the nanopillared surface structure. When coated in gold, this bactericidal effect was not inhibited, suggesting that the bacterial cell death was a result of a physical rather than chemical feature of the surface: the nanotopography.<sup>18</sup>

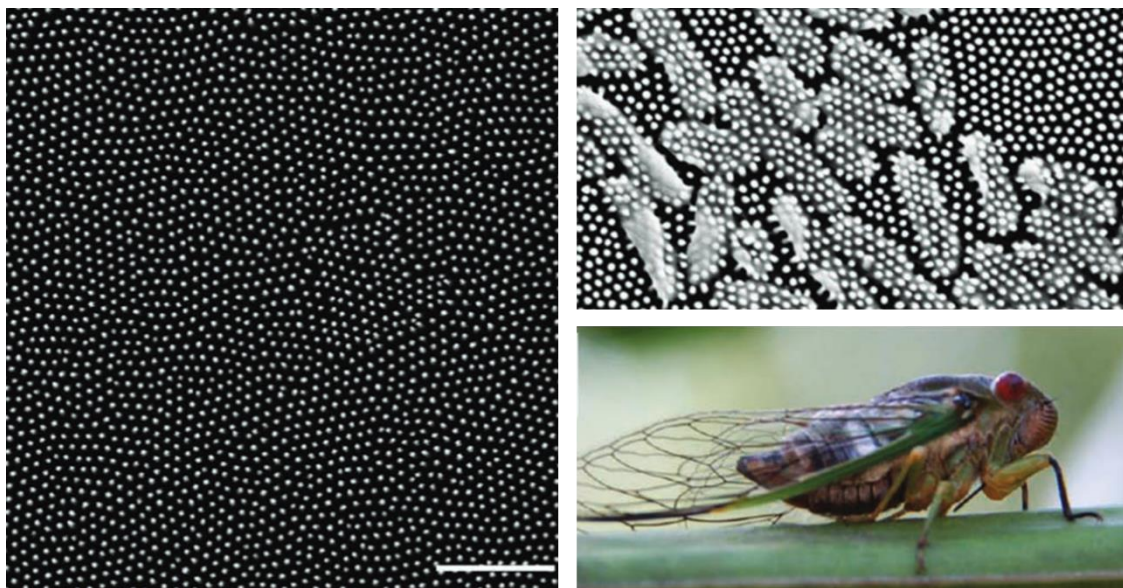


Figure 1. Bactericidal cicada wings. Left: SEM image of the hexagonally arranged nanopillars on the cicada wing. Top right: SEM image of *Pseudomonas aeruginosa* cells being penetrated on the surface of the wing. Bottom right: the *Psaltoda claripennis* species of cicada which was investigated.<sup>18</sup>

There have been similar findings with other species such as dragonflies, whose wings have a nanotopography of densely and randomly distributed cylindrical nanopillars with varying heights which

protrude from horizontal ridges on the wing. These wings were shown to be bactericidal against *Escherichia coli*, with SEM showing membrane deformation by the nanopillars.<sup>24</sup>

As well as surface structure, surface chemistry can also play a crucial role in bacterial adhesion to the surface. Generally, superhydrophobic surfaces (surfaces that have a water contact angle greater than 150°) are antibiofouling as cells cannot adhere to the surface, this is not due to any bactericidal effect.<sup>25</sup> However, some surfaces combine antifouling and bactericidal properties to act as a highly effective antibacterial surface. For example, the lotus leaf is a well-known natural superhydrophobic surface: it possesses this property due to an air cushion entrapped at the solid-liquid interface when water lands on the leaf and also due to its low energy surface wax. However, a more recent study by Jiang *et al.* has shown the surface to also be mechanically bactericidal due to a hierarchical surface structure of micro papillae and nanotubes. This combination of features makes for an extremely efficient antibacterial surface by combining antifouling and bactericidal effects.<sup>26</sup>

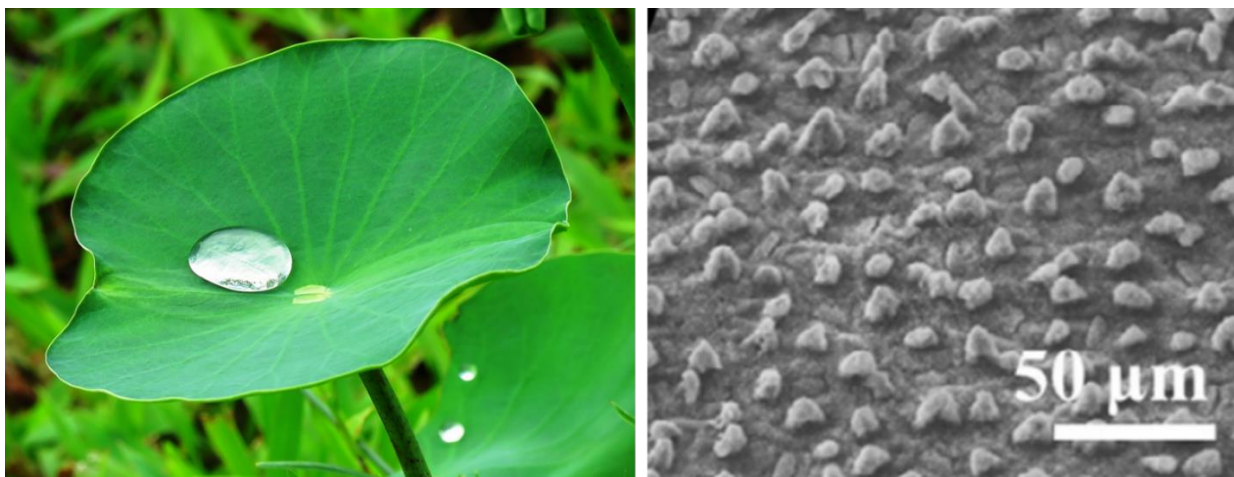


Figure 2. A lotus leaf with a superhydrophobic surface<sup>27</sup> and its nanostructured surface shown by SEM.<sup>26</sup>

This combination of properties is also seen in geckos and there have been several studies on gecko skins being used as a template for synthetic antimicrobial surfaces. Watson *et al.* investigated the skin of the box patterned gecko, showing it to have a hierarchical surface structure of micro-sized dome shaped scales and slightly curved nano hairs. The gecko skin was shown to have bactericidal properties against Gram-negative bacteria *Porphyromonas gingivalis* and was also superhydrophobic due to the surface topography.<sup>23</sup>

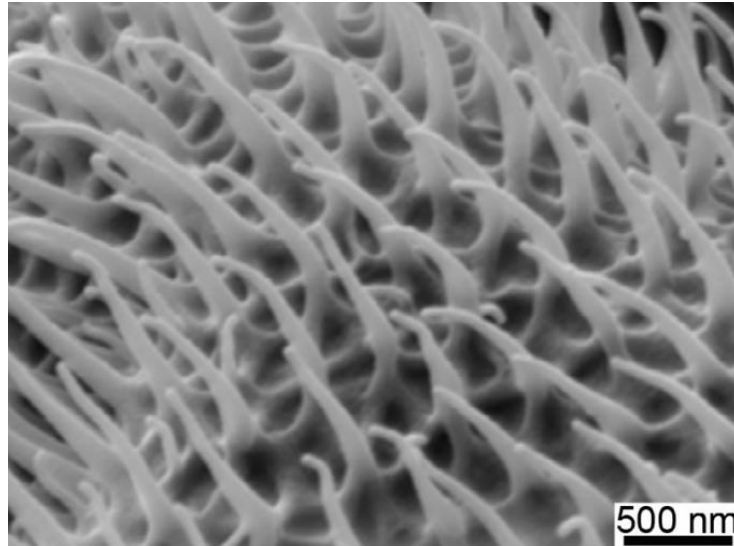


Figure 3. SEM image of the nanospinules on gecko skin.<sup>23</sup>

### 1.2.2 Physical mechanism of cell death on nanostructured surfaces

Studies of the wings of cicadae have helped to develop a model for the mechanism of cell death on this type of nanostructured surface, giving an insight into how they have their bactericidal effect and potentially enabling the optimization of this type of surface.

As previously mentioned, a study by Ivanova *et al.* found the bactericidal nature of the wing surface of *Psaltoda claripennis* to be physical rather than chemical. This was investigated by coating cicada wings in 10 nm gold film which reduced the hydrophobicity of the surface (water contact angle decreased from 158.8° to 105.5°) but did not affect the surface structure. After coating, the wing had the same bactericidal properties, indicating that the bacteria are killed by a mechanism purely based on the surface structure rather than any surface chemistry. This study further investigated the interaction between the nanopillars and the cells using confocal laser scanning microscopy (CLSM) and scanning electron microscopy (SEM). The structure of the surface was characterised in detail, showing hexagonal arrangements of nanoscale pillars 200 nm tall, 100 nm base diameter, 60 nm tip diameter, 170 nm spacing centre to centre. CLSM and SEM showed that the Gram-negative *Pseudomonas aeruginosa* cells were killed on contact with these nanoprotusions: as soon as they attached, the nanopillars began to penetrate them and killed the majority within 5 minutes. Measurements by atomic force microscopy showed that cells would move about 200 nm into the wing surface before the cell ruptured (indicated by a sudden, short downward displacement) after about 3 minutes.<sup>18</sup>

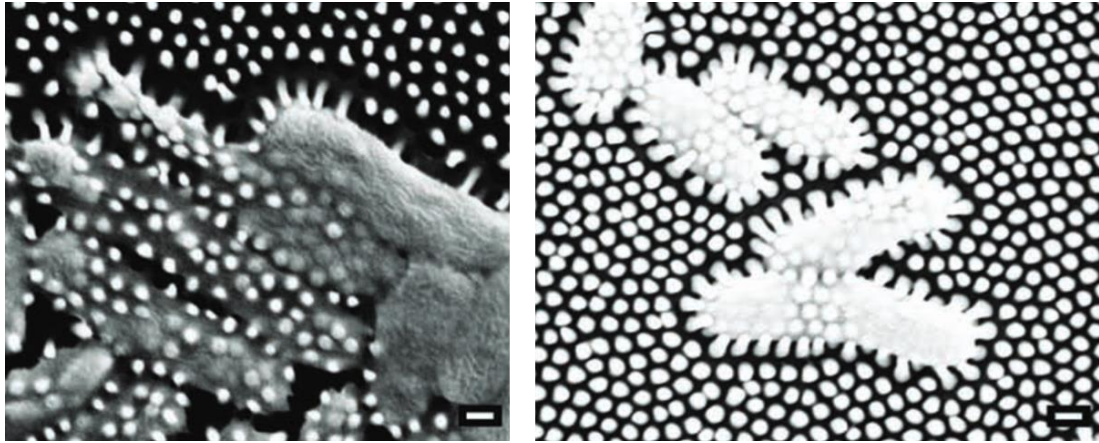


Figure 4. SEM images of *Pseudomonas aeruginosa* cells on the surface of the uncoated (left) cicada wing and gold coated (right) cicada wing.<sup>18</sup>

The cicada wing surface was further studied by Pogodin *et al.* who investigated the effect on three Gram-positive strains of bacteria (*Bacillus subtilis*, *Planococcus maritimus* and *Staphylococcus aureus*) and developed a model for the interaction between cells and the nanostructures.<sup>28</sup> Previously, the cicada wing surface was found to be effective at killing Gram-negative bacteria such as *Branhamella catarrhalis*, *Escherichia coli*, *Pseudomonas aeruginosa*, and *Pseudomonas fluorescens* while Gram-positive cells were resistant.<sup>29</sup> As Gram-positive bacteria are more rigid due to the thicker peptidoglycan layer<sup>7</sup>, this suggests that the bactericidal mechanism of the wings is more effective against cells with less rigid membranes. Results from this study further supported this theory by using microwave irradiation to decrease the membrane rigidity of Gram-positive bacteria and examine the effect this had on their susceptibility to the nanopillared surface of the cicada wing. CLSM showed that all three Gram-positive strains tested were initially resistant to the nanopillared surface but were significantly deformed and inactivated by the structure after microwave radiation, suggesting that the reduction in cell rigidity made the cells vulnerable to the nanostructures.<sup>28</sup>

This study also developed a biophysical model of the interaction between cells and the cicada wing surface structure that results in cell death. The cell membrane can be modelled as a thin elastic layer that is unevenly stretched between the pillars as the cell adsorbs onto them. At a certain point, this stretching results in the rupture of the membrane, which causes cell death.<sup>28</sup>

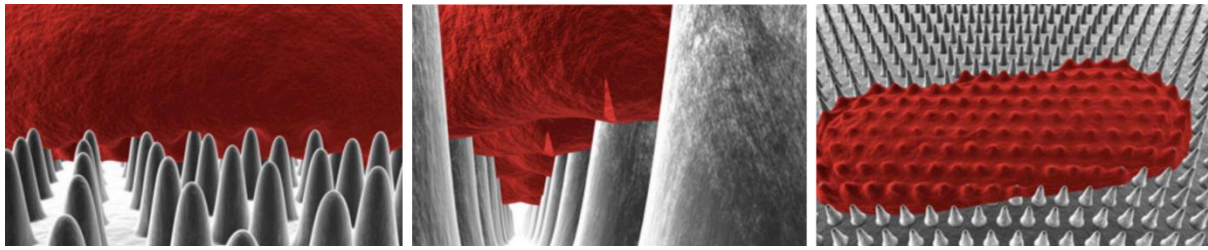


Figure 5. Three dimensional representation of the interaction between a rod shaped bacteria and the cicada wing surface: the membrane is stretched between the pillars, causing it to rupture and the cell collapses.<sup>28</sup>

It was previously thought that the part of the cell membrane suspended between nanopillars would rupture and therefore, increasing the spacing between nanopillars would increase bactericidal efficiency.<sup>28, 30</sup> However, more recent studies have found that reducing the spacing does not reduce stress and strain across the membrane and suggest that nanopillars predominantly rupture the cell membrane at the point of contact between the cell and the tip of the pillar. It is therefore fitting that increasing the number of nanopillars that a cell comes into contact with as well as reducing the tip diameter of these pillars increases rates of cell death.<sup>31</sup> This has previously been observed experimentally in studies of cicada wings<sup>25</sup> and black silicon<sup>32</sup>.

Recent studies have also shed light on additional ways that these nanostructured surfaces limit biofilm formation and bacterial proliferation. It has been found that in addition to physically deforming bacterial cells, nanopillared surfaces can induce oxidative stress and cell impedance which limits their ability to multiply and form biofilms.<sup>33, 34</sup>

### 1.2.3 Synthetic antibacterial surfaces

Natural antibacterial surfaces have inspired a series of synthetic antibacterial surfaces, often based on the nanotopography of the natural surface but made from different materials. Materials that have previously been used include several metals<sup>35, 36</sup>, polymers<sup>37</sup>, diamond<sup>38</sup> and black silicon<sup>39</sup>. Studies on various materials with different nanostructures allows conclusions to be made about the structural characteristics that make the surface more effective in order to improve future designs.

An antibacterial surface that mimics the surface of dragonfly wings was produced by etching a nanowire structure onto titanium using a hydrothermal etching technique. SEM observed nanowire arrays arranged mainly in perpendicular configuration to each other on the surface of the hydrothermally etched titanium and the nanowires were approximately 40.2 nm tall. Bacterial attachment was investigated on this surface and compared to the flat titanium surface using Gram-positive *Staphylococcus aureus* and Gram-negative *Pseudomonas aeruginosa*. There was greater bacterial attachment on the unetched titanium surface. On the etched surface, a greater number of the Gram-negative *Pseudomonas aeruginosa* cells appeared to be damaged by the nanowires on the surface

(80.2% of the *S. aureus* and 52.9% of the *P. aeruginosa* cells remained viable after attachment), as tends to be the case when the destruction of the cell relies on physical disruption of the membrane due to the thinner peptidoglycan layer in Gram-negative bacteria. For the etched surface, there was less bacterial attachment and the surface appeared to be made moderately bactericidal by the nanowires.<sup>35</sup>

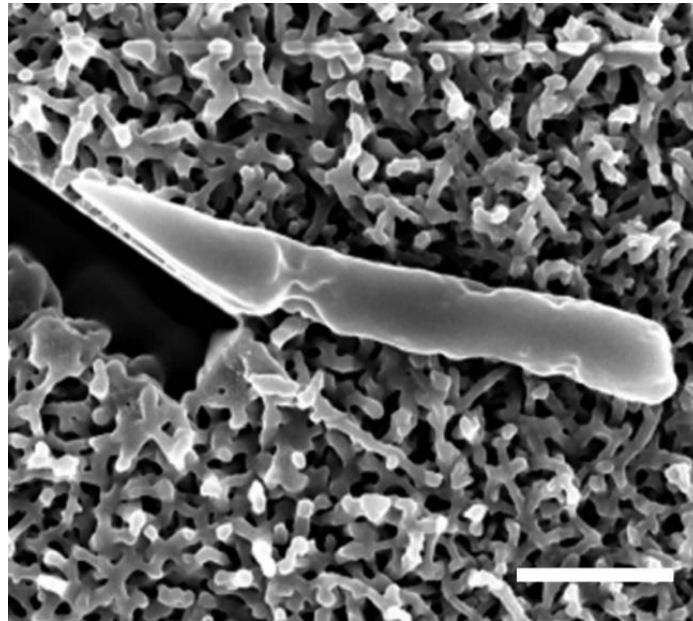


Figure 6. *P. aeruginosa* cell interacting with nanowires on hydrothermally etched titanium surface.<sup>35</sup>

Gold nanostructured surfaces were used to investigate the effect of some different shaped nanostructures of similar sizes on Gram-positive bacteria methicillin-resistant *Staphylococcus aureus* (MRSA). Three types of gold nanostructured surfaces were produced by electrodeposition on nanoporous alumina templates: nanopillars, nanorings and nanonuggets. These features were all about 100 nm in height and nanopillars about 50 nm diameter and nanorings and nuggets about 200 nm diameter. When the attachment of MRSA was tested and compared to flat surfaces, it was found that the nanostructured surfaces were very effective antibacterial surfaces: less than 1% of the number of cells found on flat/rough surfaces were found on the nanostructured surfaces. SEM showed mechanical deformation of cell membranes on the surfaces. Additionally, cell proliferation experiments showed that the number of live *S. aureus* cells was 3 times lower on the Au nanostructured surfaces than on flat/rough reference surfaces.<sup>36</sup>

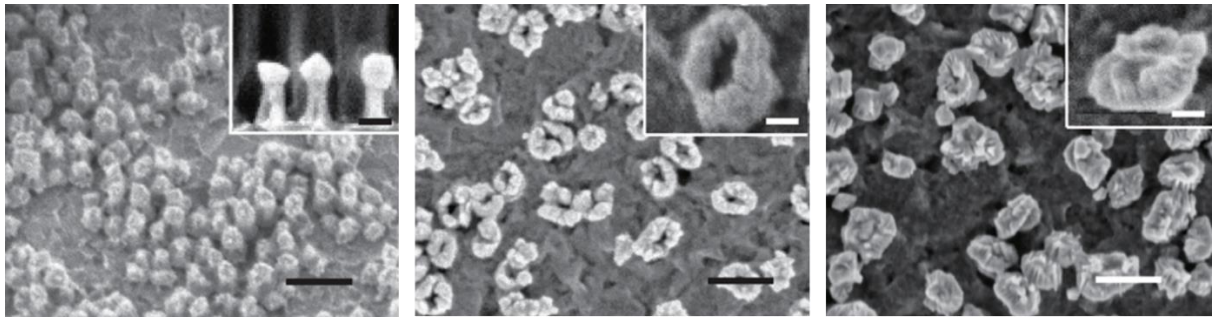


Figure 7. SEM images of gold nanopillars, nanorings and nanonuggets (left to right).<sup>36</sup>

Another biomimetic surface based on the nanopillars of cicada wings was produced using poly(methyl methacrylate), a polymer that is approved and used in medical devices. In this study, nanopillar arrays of different sizes and spacing were produced and investigated. As expected, more dead bacteria were observed on the pillared films than on flat control films but results also demonstrated the importance of the dimensions of the features. More dead bacteria were observed on the films with narrower pillars with smaller spacing: this significantly decreased with increasing pillar size and spacing.<sup>37</sup> These results fit predictions from recent models which show that smaller pillars apply more local stress to cell membranes and more contact points between nanofeatures and the bacterial cell increase disruption to cells and therefore rates of cell death.<sup>31</sup>

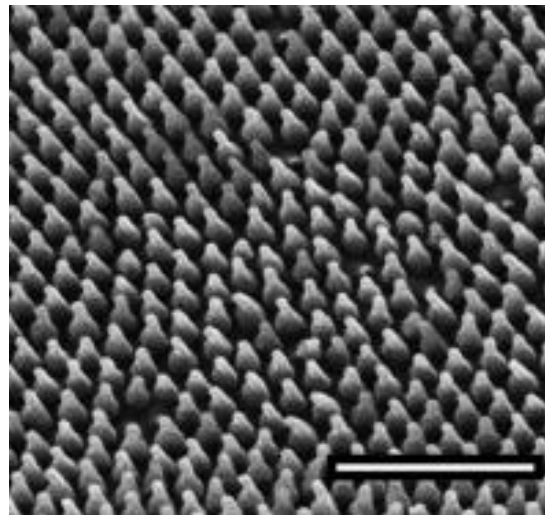


Figure 8. Micrograph image of poly(methyl methacrylate) replication of cicada wing surface.<sup>37</sup>

The effect of the dimensions of nanostructures was also investigated with diamond nanocone surfaces, again inspired by cicada wings. This study used Gram-negative *Pseudomonas aeruginosa* to investigate

and compare the bactericidal activity of two different diamond nanocone surfaces: A and B. The properties of surfaces A and B are shown in Table 1 and Figure 9.

Table 1. Properties of diamond two diamond nanocone surfaces A and B.<sup>38</sup>

	Surface A	Surface B
Cone height	800 nm to 2.5 $\mu\text{m}$ Average height: 1.65 $\mu\text{m}$	<100 nm 3-5 $\mu\text{m}$
Cone width	350-750 nm	<100 nm-1.2 $\mu\text{m}$
Tip diameter	10-40 nm	10-40 nm
Cone density	$4 \times 10^8 \text{ cm}^{-2}$	$1.7 \times 10^8 \text{ cm}^{-2}$

Both surfaces were significantly more effective than the control flat silicon wafer but surface B was 17% more lethal than surface A. This paper hypothesized that the sharp tips of the nanocones would induce stress across the bacterial cell wall on contact and this would cause the cells to stretch, puncture and lyse, causing the bacterial cell to die. The nonuniformity of surface B appeared to damage a greater proportion of cells.<sup>38</sup>

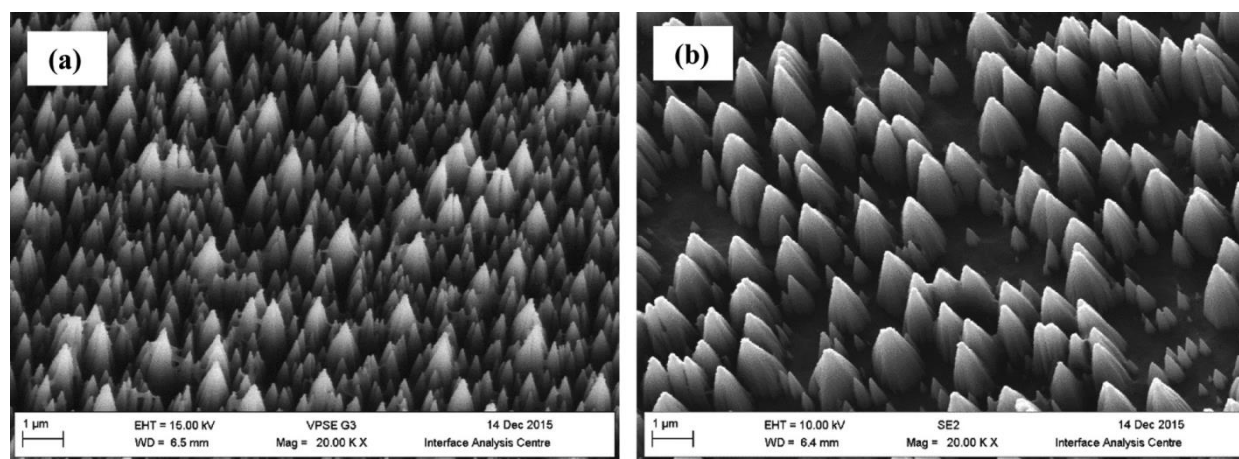


Figure 9. SEM images of diamond nanocone surfaces A (left) and B (right).<sup>38</sup>

For the first time, antiviral activity was investigated on a nanostructured surface. An aluminium alloy surface with 23 nm wide nanostructures arranged randomly in ridges was produced using a wet etching technique. The surfaces produced were shown to be hydrophilic and increased etching time increased the nanoscale roughness of the surface. These surfaces were tested with the Gram-negative bacteria *Pseudomonas aeruginosa* and the Gram-positive bacteria *Staphylococcus aureus* and also two common

viruses: respiratory syncytial virus (RSV) and rhinovirus (RV). Both bacterial strains were physically deformed and after 3 hours were not viable: 92 and 87% of *P. aeruginosa* and *S. aureus*, respectively were inactivated by the surface. The effect of the surface on both RSV (enveloped) and RV (nonenveloped) were investigated and compared to a flat Al surface and cell culture plastic. While RSV viability naturally reduces over time, the nanostructured surface increased the rate of this decline, with much lower levels of live viable virus remaining on the nanostructured surface than the flat surfaces after 2 hours. However, it seemed to be more effective against the nonenveloped rhinovirus (RV), with only the nanostructured surface reducing the viability of this virus and leaving virtually no virus viable after 24 hours. While these are promising results, the mechanism of this effect has not been investigated yet but it is unlikely to be the same as bacteria as viruses do not move and their lipid envelopes are thinner and less flexible.<sup>40</sup> While the majority of the research up to this point has been on surfaces that kill bacteria, the possibility of a surface that is also lethal to viruses is an exciting development that would improve the effectiveness of this type of surface.

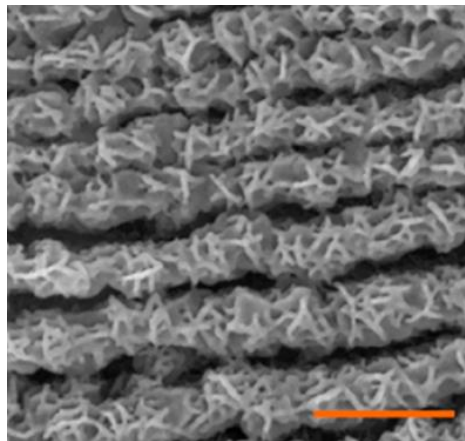


Figure 10. SEM image of 3 h wet etched titanium with random nanostructures.<sup>40</sup>

### 1.3 Black silicon (bSi)

A material of particular interest is black silicon: the surface of this material is covered in high aspect ratio nanoprotusions and absorbs over 99% of visible light, giving it its characteristic deep black colour.<sup>32</sup> Originally produced as a side product of reactive ion etching (RIE), this material can be produced using various techniques and the physical properties vary depending on the production method. Due to its low surface reflectance, black silicon is used in applications such as solar cells, photodetectors and photodiodes.<sup>41</sup>

However, more recent research has shown that the characteristic nanoprotusions also give the material bactericidal properties, the nanotopography is similar to structures found in nature which are shown to

have a bactericidal effect such as the wings of cicada and dragonfly. In black silicon, nanoprotusions on the surface kill bacterial cells *via* a physical mechanism as previously discussed. A study by Ivanova *et al.* investigated the antibacterial activity of this surface and compared it with that of the wing of the *Diplacodes bipunctata* species of dragonfly and the previously studied cicada wing surface. To investigate this effect, both Gram-negative (*Pseudomonas aeruginosa*) and Gram-positive (*Staphylococcus aureus*) bacteria were tested as well as the vegetative cells and spores of *Bacillus subtilis*: both the black silicon and dragonfly wings showed similar bactericidal activity against all the strains tested. In this study, it was shown that the killing rate for both surfaces over the first 3 h was  $\sim 450,000$  cells  $\text{min}^{-1}\text{cm}^{-2}$ , this declined to  $50,000$  cells  $\text{min}^{-1}\text{cm}^{-2}$  for *S. aureus*. For reference, the minimum infective doses are  $10^3$  cells for *P. aeruginosa* and  $10^5$  cells for *S. aureus* so these surfaces kill a significant amount of bacteria to be antibacterial surfaces.<sup>39</sup>

As previously discussed, varying certain properties of a nanostructured surface affects its bactericidal efficacy. A paper by Hazell *et al.* investigated the antibacterial efficacy of black silicon and black diamond surfaces with varying needle length, areal density and sharpness. While several factors were important, it was found that the areal density of the needles was found to be the most significant factor affecting the bactericidal efficacy of the surface, with increasing density (smaller spacing) seeming to increase the bactericidal efficacy of the surface.<sup>32</sup> This supports findings that the more nanostructures with which the cells come into contact, the greater the bactericidal effect of the surface.<sup>25</sup> With regards to the length of the needles, it seems that there is a lower limit at which it becomes effective and beyond that, the death rate increases with increasing needle length up to an upper limit at which there seems to be no further effect as maximal stretching of the cell membrane has already occurred. Additionally, the smaller the diameter and pitch of the nanopillars, the greater the bactericidal effect of the surface.<sup>32</sup>

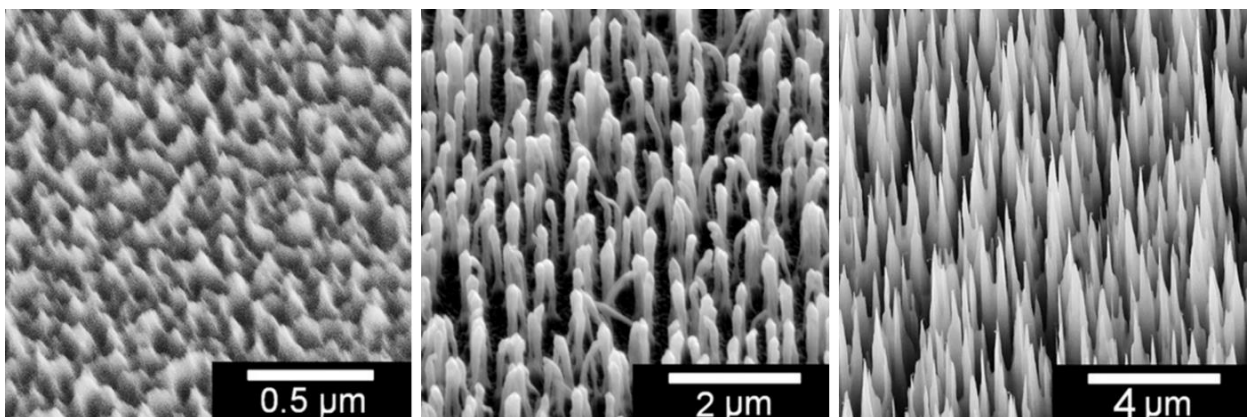


Figure 11. SEM images of black silicon with different needle lengths (increasing left to right).<sup>32</sup>

## 1.4 Black diamond (bD)

While black silicon has been shown to act as a mechanically bactericidal surface, this material has the disadvantage of being extremely fragile: even a fingernail can cause the needles to break. Coating the black silicon surface in diamond using chemical vapour deposition not only makes it less fragile, but it also gives the option of functionalising the surface by altering the surface termination of the diamond which affects the hydrophobicity or hydrophilicity. This can be done via a chemical treatment or by exposing the diamond to a reactive plasma.<sup>42</sup>

Coating the black silicon needles in diamond results in slightly less ‘sharp’ and more rounded needles with the tip radius increasing from ~30 nm to ~300 nm on coating with diamond. The average needle length was also reduced by ~1.5  $\mu\text{m}$  due to etching during the deposition process.<sup>42</sup> The slightly altered properties of the nanoprotusions does not seem to negatively affect the bactericidal activity of the black diamond versus the black silicon. Studies using *Escherichia coli* and *Streptococcus gordonii* showed that in fact, the death rate for black diamond needles is slightly higher than for black silicon needles.<sup>32</sup>

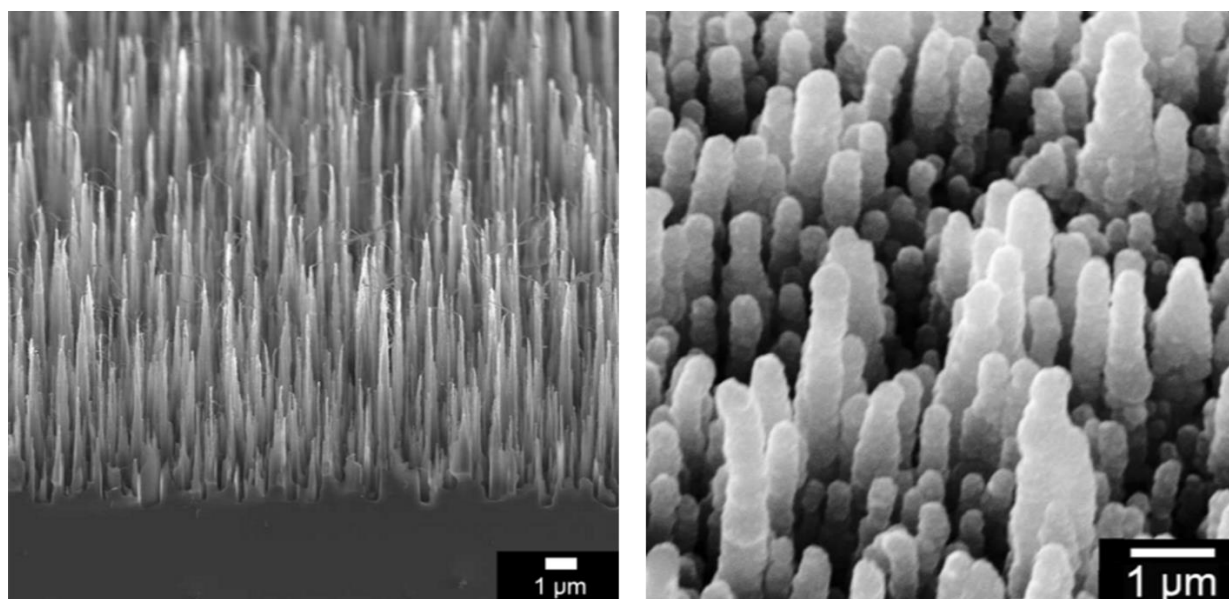


Figure 12. SEM images of black silicon before and after coating with diamond.<sup>42</sup>

An additional benefit of coating the black silicon needles with diamond is that the surface termination can be altered to change the physical properties such as hydrophobicity. As seen from various natural and synthetic antibacterial surfaces, altering the hydrophobicity of the surface can change the antibacterial effect. While terminating the surface with fluorine makes the surface negatively charged and hydrophobic, terminating with oxygen makes it more hydrophilic.<sup>43</sup>

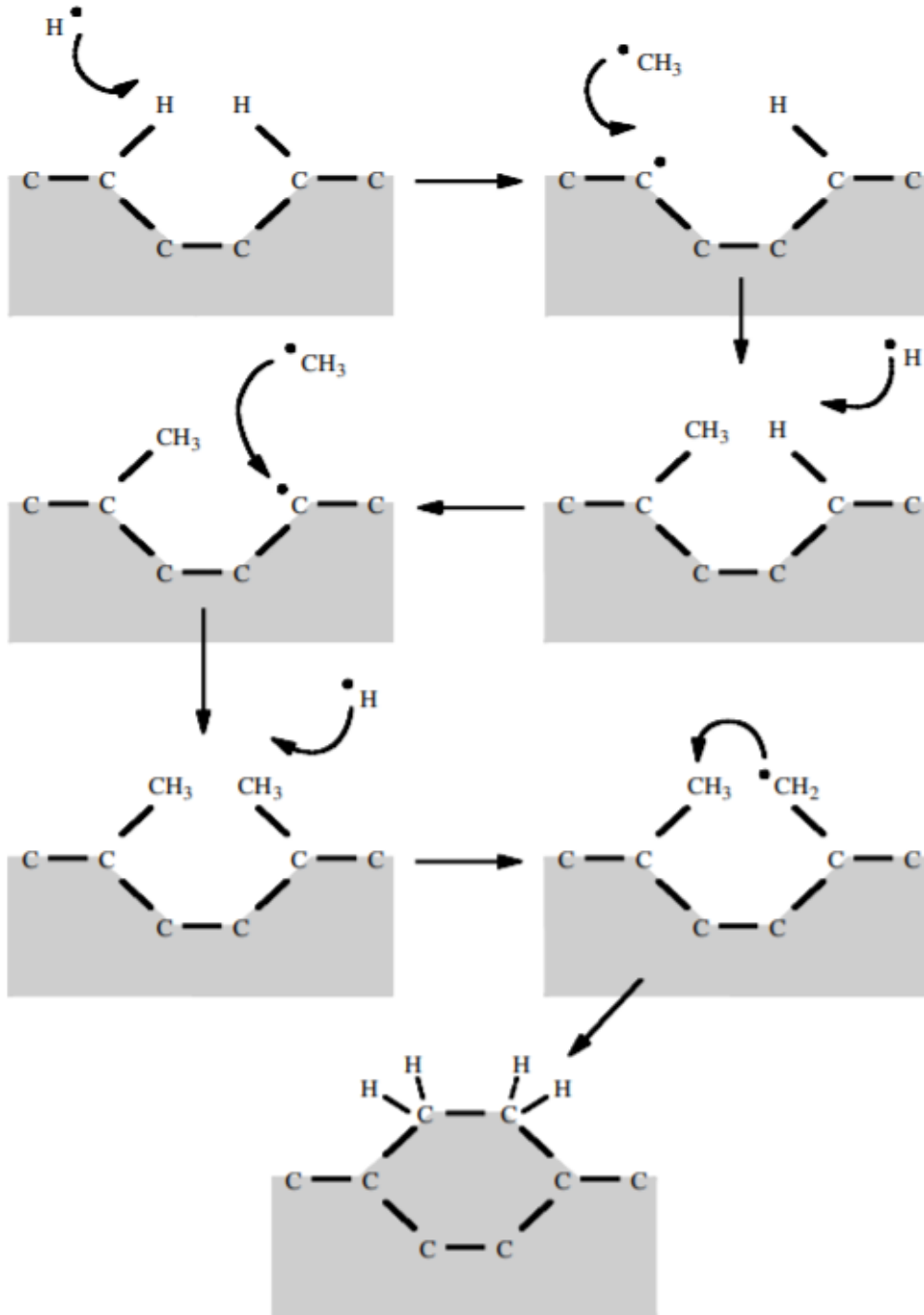
A study by Dunseath et al. investigated the effect of different surface terminations of black diamond on the bactericidal efficiency of the surface against Gram-negative *E. coli*. Black diamond surfaces terminated with H, NH<sub>2</sub>, O and F (in order of increasing hydrophobicity) were tested. Unsurprisingly, for the H, NH<sub>2</sub> and O terminated surfaces, increasing hydrophilicity of the surface increases the number of bacteria that stick to the surface, but a smaller proportion are killed on contact. Conversely, F terminated black diamond is hydrophobic with a contact angle of 137.0° and unexpectedly, was shown not to reduce bacterial adhesion but did increase the proportion of adhered cells killed. This suggests that surface termination is not actually very effective at preventing bacteria from adhering but hydrophobicity can enhance the bactericidal effect.<sup>42</sup>

### 1.4.1 Diamond

Diamond is an allotrope of carbon with numerous remarkable properties which make it an invaluable material in a range of applications. Some noteworthy properties of diamond are its extreme hardness and strength, high thermal conductivity, good electrical insulating ability, optical transparency between UV and IR wavelengths and its resistance to chemical corrosion. However, despite this exceptional range of properties, diamond is used less than one might expect due to its natural scarcity.<sup>44</sup>

Natural diamond is formed at high pressure and temperature deep underground in the earth mantle and initial methods of producing synthetic diamond were based on recreating these conditions. The high-pressure high-temperature (HPHT) growth technique involves compressing graphite in a hydraulic press to very high pressure and temperature so that diamond forms from the graphite.<sup>45</sup>

A more recent development is the chemical vapour deposition (CVD) method which involves a gas phase reaction of a hydrocarbon, usually methane, in an excess of hydrogen which results in deposition onto a solid substrate. This reaction requires activation of the carbon-containing molecules, which can be achieved by several methods such as a hot filament or electric discharge. While the gas-phase chemistry of this process is very complex and there are additional factors to consider, a proposed basic mechanism is described here. Gases (~1 % methane in hydrogen) are introduced into the reaction chamber and are energized and fragment into highly reactive radicals as they pass through the ‘activation region’. As shown in Scheme 1, an H radical can react with a surface H, forming H<sub>2</sub> and leaving a reactive carbon site on the surface. This reactive site will either react with another H, resulting in no change or occasionally a CH<sub>3</sub> radical will react and add a carbon atom to the lattice. If this process repeats at an adjacent site, a ring structure can be formed as further radical reactions occur as shown and the newly added carbon atoms are locked into the lattice, resulting in diamond being formed if the conditions are right.<sup>45</sup>



Scheme 1. Proposed reaction scheme of how  $\text{CH}_3$  radicals add to the diamond lattice.<sup>45</sup>

The H radicals formed are also essential for several processes which result in higher quality diamond being formed. Firstly, H radicals quickly react at excess ‘dangling bonds’ that are generated during the reaction and prevent graphitization from occurring. Additionally, H atoms can etch both diamond-like  $\text{sp}^3$  carbon and graphitic  $\text{sp}^2$  carbon but etch  $\text{sp}^2$  carbon at a faster rate, therefore removing graphene that forms on the surface and leaving the diamond.<sup>45</sup>

Diamond does not spontaneously grow on non-diamond surfaces, therefore either diamond must be used as the substrate, or the substrate must be treated to enable nucleation.<sup>46</sup> This can be done by seeding with nanodiamonds or mechanical abrasion of the substrate to create scratches which act as growth templates.<sup>45</sup>

### **1.4.2 Surface Termination**

While diamond growth by chemical vapour deposition is typically hydrogen terminated, altering the surface termination of the diamond can alter the properties which can have important effects on its applications, including in antibacterial surfaces as explored earlier.

For example, oxygen and amine terminated surfaces will be more hydrophilic<sup>47</sup> whereas a fluorine terminated surface will be more hydrophobic<sup>43</sup>. Oxygen, fluorine and amine terminations can be achieved by bombardment of the diamond surface with ions of the desired terminating species by exposing it to a plasma of oxygen, ammonia or sulphur hexafluoride gas, respectively.<sup>43, 48</sup>

There are many more examples of surface termination of diamond using various elements and their functional groups which can facilitate covalent grafting of biological molecules and other applications.<sup>49</sup> Combining nanostructured surfaces with this kind of functionalization could be an interesting development in antimicrobial surfaces in the future.

## 1.5 Previous Work

Previously, black silicon has been studied as an antibacterial surface by various groups. Studies have shown the material to be effective against both Gram-positive and Gram-negative bacteria.<sup>39</sup> However Gram-negative bacteria were generally more affected by this type of nanostructured surface and some studies have even observed black silicon to have no significant effect against Gram-positive bacteria.<sup>32</sup>

Black diamond has been studied within the diamond group at Bristol, to examine the effect of the diamond coating on the biocidal activity of black silicon surfaces in terms of the dimensions of the needles and surface termination. Gram-negative bacteria *Escherichia Coli* has been shown to be significantly affected by black diamond with different needle lengths ranging from 1.0-20  $\mu\text{m}$  long, with death rates of *E. Coli* on the surface being  $\sim 20\%$  higher than on flat diamond control samples. These death rates were also slightly higher than those of *E. Coli* on corresponding black silicon surfaces with similar dimensions.<sup>32</sup>

However, so far Gram-positive bacteria have been shown to be unaffected by black diamond surfaces, with death rates of  $\sim 1.5\%$  observed for Gram-positive bacteria *Streptococcus Gordonii* on black diamond surfaces.<sup>32</sup>

Termination of the diamond surface has also been altered in various ways, with results of bacterial testing showing that bactericidal activity generally increased with increasing hydrophobicity. For example, fluorine terminated black diamond surfaces killed  $\sim 50\%$  of adhered *E. Coli* bacteria compared to  $\sim 33\%$  for equivalent hydrogen terminated black diamond surfaces.<sup>42</sup>

More recently, more tests of Gram-positive bacteria on black diamond surfaces have been carried out using *Staphylococcus aureus* but this has been limited up to this point.

## 1.6 Project Aims

The aim of this project was to build on the previous work done on black silicon and black diamond as antimicrobial surfaces against Gram-positive bacteria as there has been limited investigation of this to date. We planned to prepare a set of identical black diamond samples to be sent to Groningen University in the Netherlands where they will undergo bacterial viability testing using two species of Gram-positive bacteria *Staphylococcus aureus* and *Staphylococcus epidermidis*.

Only one type of black silicon will be used in this project as limited lab time will limit the number of samples we are able to produce and it is more desirable to obtain reproducible results than a greater range of samples in this case.

## 2 Methodology

### 2.1 Sample preparation

#### 2.1.1 Black silicon

Black silicon wafers were obtained from LAM Technologies and cleaved into  $\sim 1 \text{ cm}^2$  squares, using a diamond tipped scribe, before being used.

#### 2.1.2 Seeding

Seeding suspensions were made up by diluting detonation nanodiamond (particle size  $3.3 \pm 0.6 \text{ nm}$ , 2.0 % weight to volume in water) in 30 mL methanol. Each suspension was sonicated using an ultrasonic probe to break up aggregations of particles that formed in suspension.

Multiple seeding suspensions were made up, using different amounts of detonation nanodiamond (DND) and different sonication times to vary the concentration of nanodiamond particles in suspension. The details of the suspensions (at time of seeding) are shown in Table 2.

*Table 2. Details of seeding suspensions used.*

Suspension	Number of drops of DND	Total sonication time at time of seeding / minutes
1	10	120
2	10	180
3	10	90
4	15	90
5	10	210
6	10	270
7	10	285

Black silicon samples were seeded by submersion in the prepared seeding suspension for one hour and then air dried for 10 minutes to allow the methanol to evaporate.

#### 2.1.3 Diamond growth

A hot filament chemical vapour deposition (HFCVD) reactor was used to grow the diamond film on the black silicon samples. Filaments were made from tantalum wire and the seeded black silicon samples were put into the reactor, lying flat just below the filaments.



*Figure 13. Black silicon samples below tantalum wire filaments.*

The reaction chamber was sealed and put under vacuum, allowing the pressure to decrease to about  $10^{-2}$  Torr. The substrate heater was then turned on (4 A) and the reactor left to pump down while the substrate heater heated up for a further 30 minutes until the pressure decreased to between  $(6-9) \times 10^{-2}$  Torr.

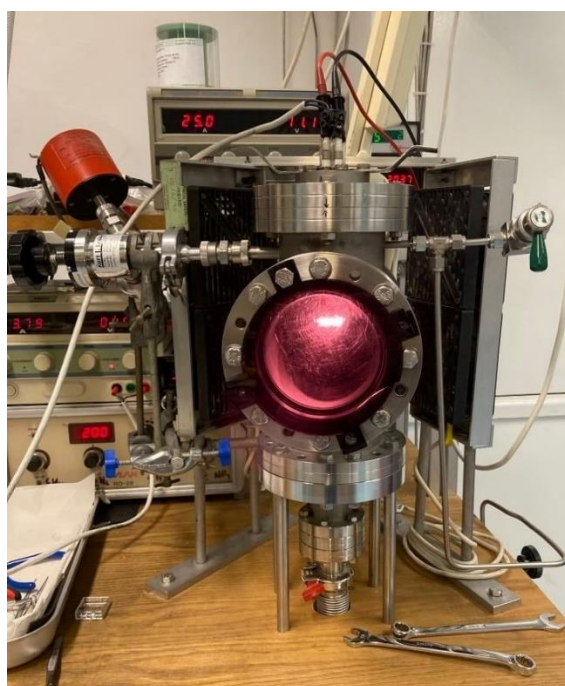


*Figure 14. Hot filament reactor during a growth run.*

Gas flow (~1 % methane in hydrogen) into the chamber was started: 2 sccm flow of methane, 200 sccm flow of hydrogen and the chamber pressure was adjusted to 20 Torr. Once the pressure and gas flows had stabilised, a 25 A current was applied to the tantalum filaments and the reactor was left for the required growth time. At the end of the growth, the filament and substrate heater power supplies were turned off and the gas flows were stopped, the reactor pumped back to base pressure, and left to cool down for 30 mins, before the chamber was vented and the samples retrieved.

## **2.2 Characterisation of samples**

### **2.2.1 Scanning Electron Microscopy**

Samples were analysed using scanning electron microscopy in order to obtain images of the nanostructures. Black diamond samples were broken in half before being mounted onto 70 ° angled stubs, so that the image taken would be of the middle of the sample instead of potentially overgrown areas around the edge.

### **2.2.2 Raman Spectroscopy**

Raman spectra of samples were taken using the 514 nm green laser of a Renishaw Raman Spectrometer with ~30 mW power, to check the quality of the diamond grown on the substrates. For each sample, 10 accumulations of 6 second spectra acquisitions were taken, with cosmic ray removal. For the black diamond samples, 10% of the power was used. However, for black silicon this was increased to 33% due to the high absorption of light of this material.<sup>32</sup>

## **2.3 Fragility test**

To test the fragility of black diamond compared to black silicon, a simple experiment was designed in which polyimide film electrical tape was applied to one half of a sample then removed after 10 minutes. The surface of the sample on both sides was checked for damage and compared using SEM. Due to the fragility of the black silicon needles, it would be expected that the tape would pull a significant number of them off.

## 3 Results and Discussion

### 3.1 Optimising seeding and growth time

It was proposed that a set of identical black diamond samples should be prepared to be used for biological testing. It is important that the samples produced have a good coating of diamond while still retaining their original shape. Due to the physical mechanism by which this type of surface kills bacteria, it is important that spacing between the needles is also retained to allow for stretching and rupture of the membranes of bacteria which adsorb onto the surface. Other dimensions of the needles such as height and width are also important, as they also affect how effective the surface is, as described previously.

Initially, black silicon samples were seeded with Suspension 1 (see Table 2) and grown in the hot filament reactor for a range of different growth times. SEM images of these samples were taken to analyse and compare the quality of the diamond coating and are shown in Figures 15-21.

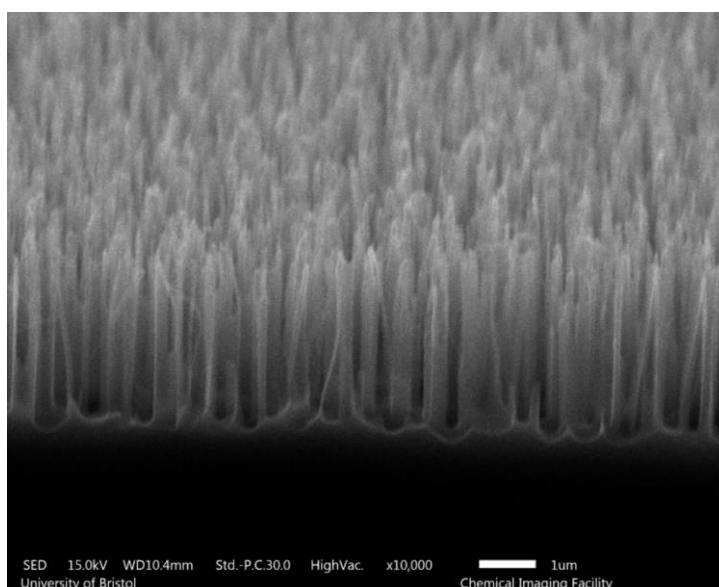


*Figure 15. SEM image of black silicon, without seeding or growth.*

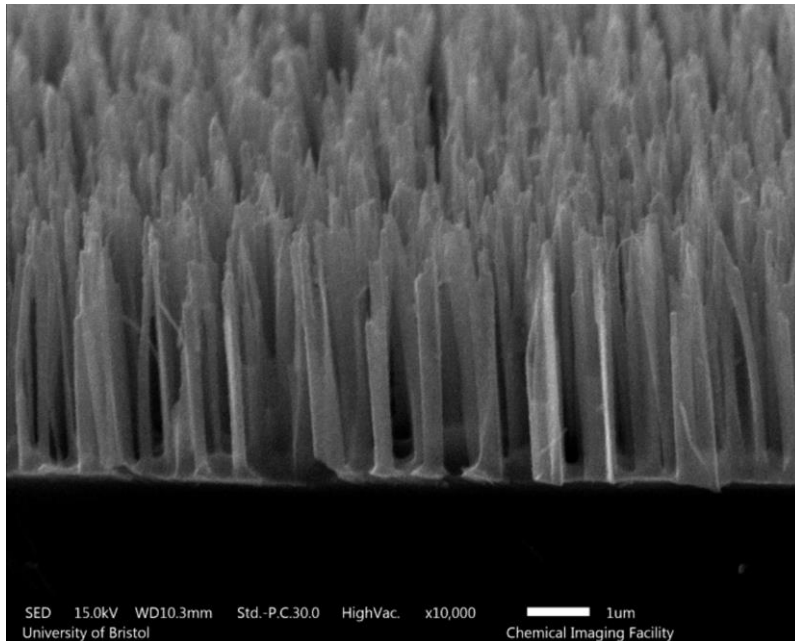


*Figure 16. SEM image of black diamond: seeding suspension 1, 10 minute growth.*

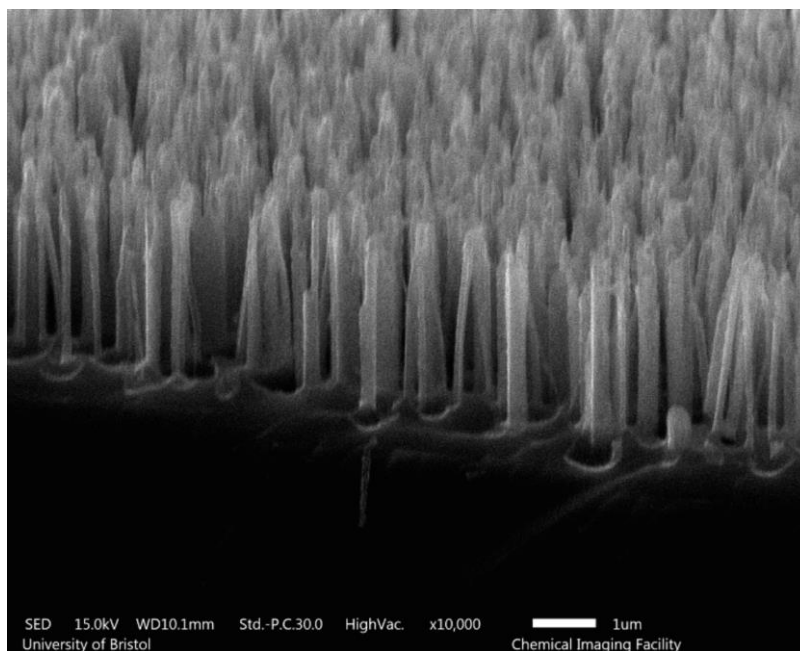


*Figure 17. SEM image of black diamond: seeding suspension 1, 15 minute growth.*

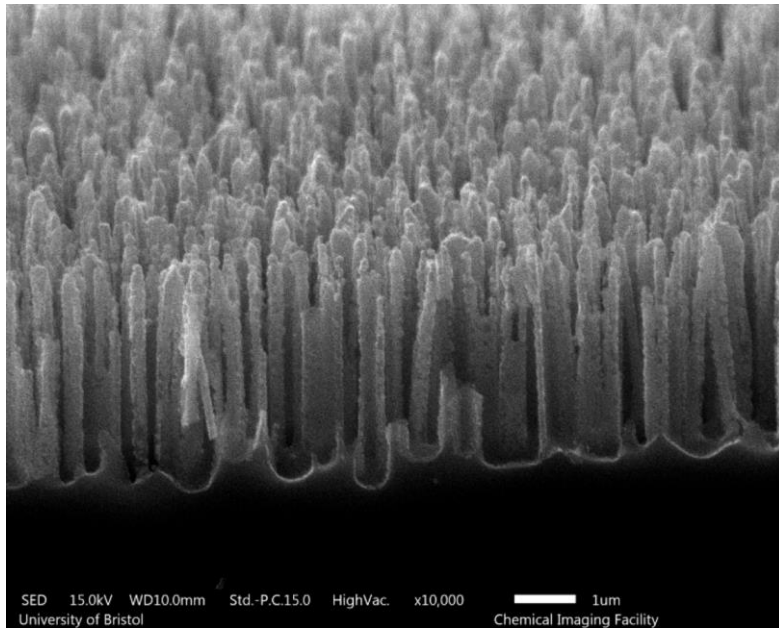


Figure 18. SEM image of black diamond: seeding suspension 1, 20 minute growth.

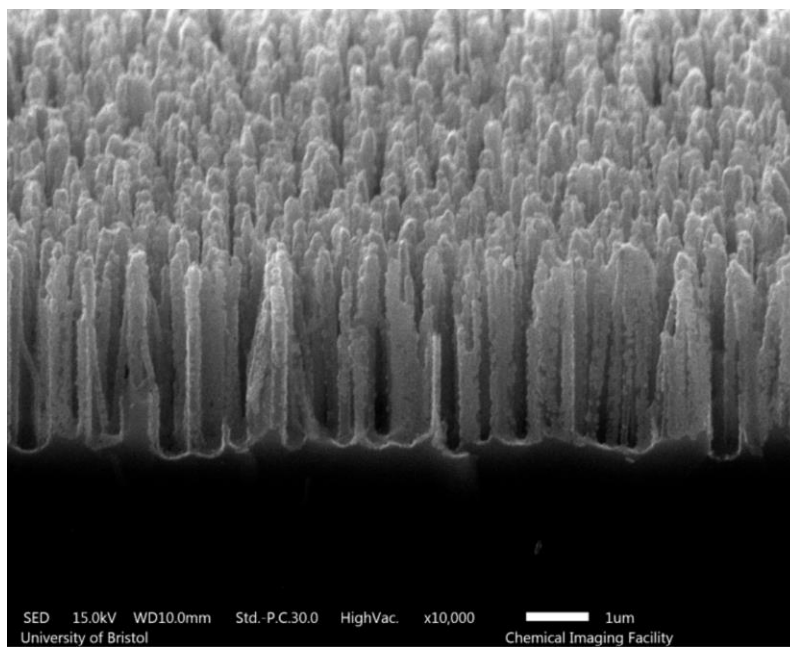


Figure 19. SEM image of black diamond: seeding suspension 1, 30 minute growth.

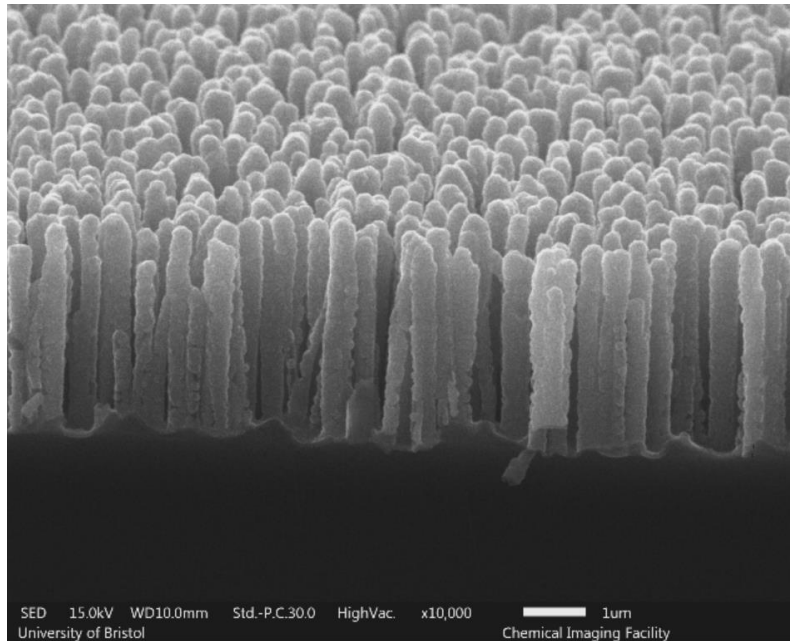


Figure 20. SEM image of black diamond: seeding suspension 1, 40 minute growth.

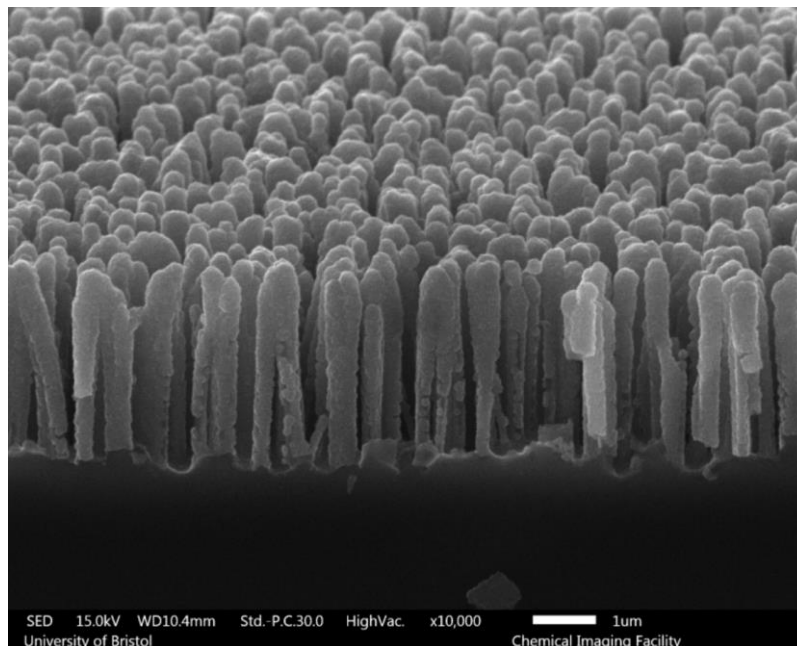


Figure 21. SEM image of black diamond: seeding suspension 1, 50 minute growth.

Visually, it can be seen that the properties of the needles changed with increasing growth time. The black diamond from longer growth times appeared to have better quality coating down the entire needles. As shown in Figure 22, the width of the needles also increased with increasing growth time as a thicker diamond film was deposited.

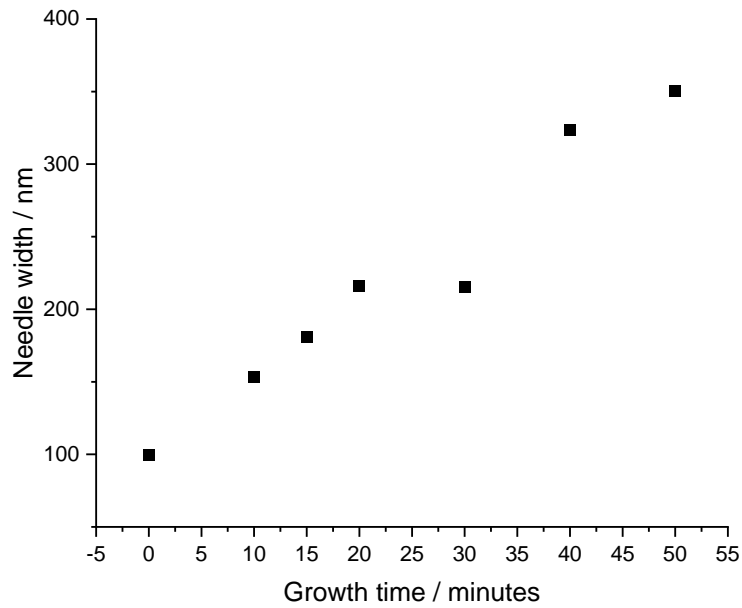


Figure 22. The width of the needles increased with longer growth times due to the thicker diamond film deposited.

However, compared to previous studies in which black diamond has been produced using this method, the samples produced here do not seem to be consistent with black diamond produced using similar methods and growth times. For example, in a previous project, black silicon with needles of a similar size was used and 40-minute growth in the hot filament reactor produced black diamond which appeared a lot more overgrown and had lost a lot more of its original nanostructure.<sup>50</sup>

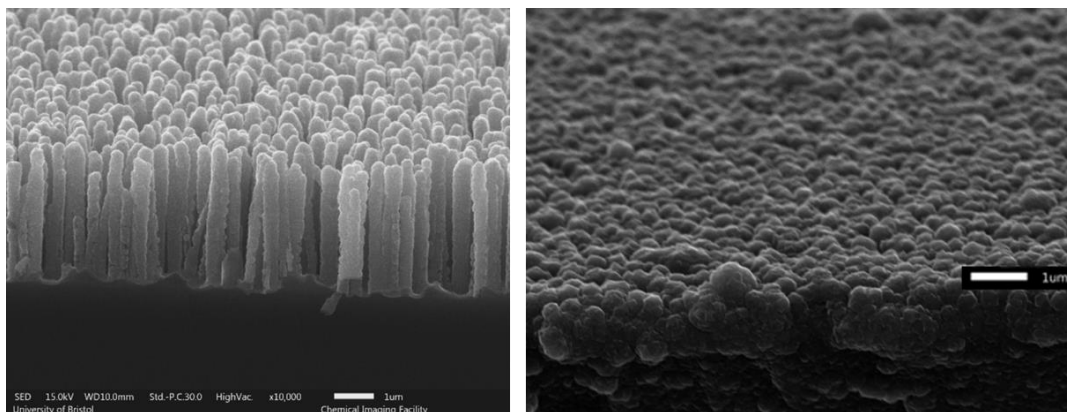
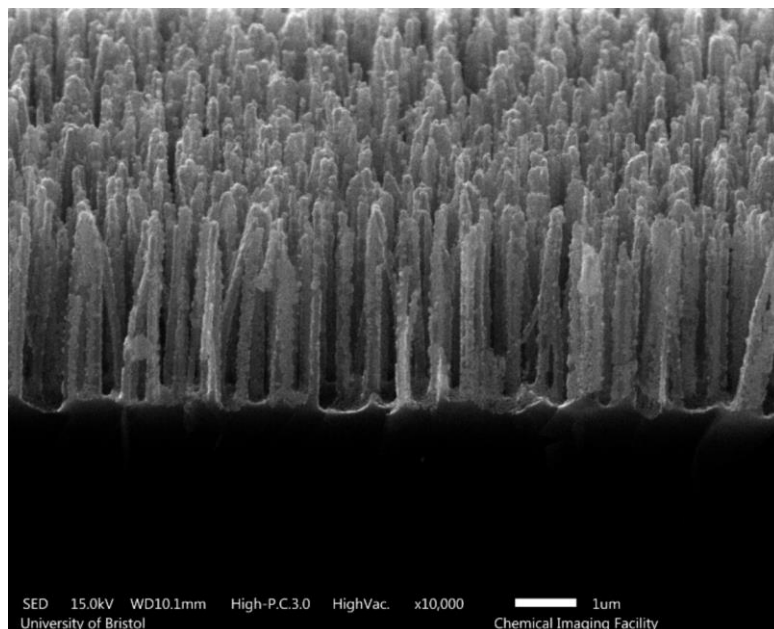


Figure 23. Black diamond samples after 40 minutes of growth in the HF-CVD reactor: the sample produced for my project (left) and a sample produced in a previous project (right).<sup>50</sup>

Due to this significant disparity between the black diamond samples produced here and samples produced previously, it was concluded that there was potentially an issue with the seeding method used for the black silicon samples. Therefore, it was decided to alter the seeding suspension by changing the concentration of DND in suspension and the sonication time of the seeding suspension.

The original 10 drop seeding suspension was sonicated for another hour (suspension 2) and two new seeding suspensions were made up using 10 (suspension 3) and 15 drops (suspension 4) of DND, 30 mL of methanol and sonicated for 1.5 hours. Black silicon samples seeded with each new seeding suspension were grown for 15 and 20 minutes in the hot filament reactor and SEM images were taken for analysis.



*Figure 24. SEM image of black diamond: seeding suspension 2, 15 minute growth.*

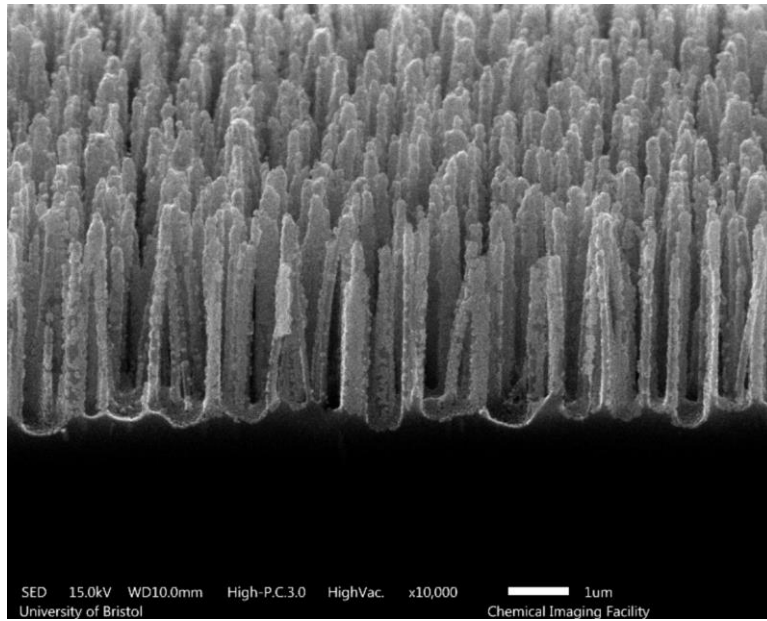


Figure 25. SEM image of black diamond: seeding suspension 2, 20 minute growth.

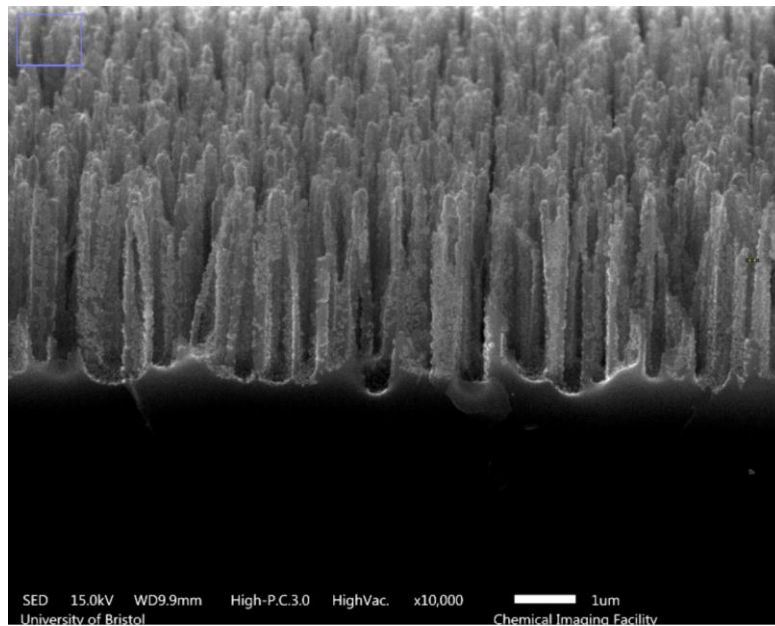


Figure 26. SEM image of black diamond: seeding suspension 3, 15 minute growth.

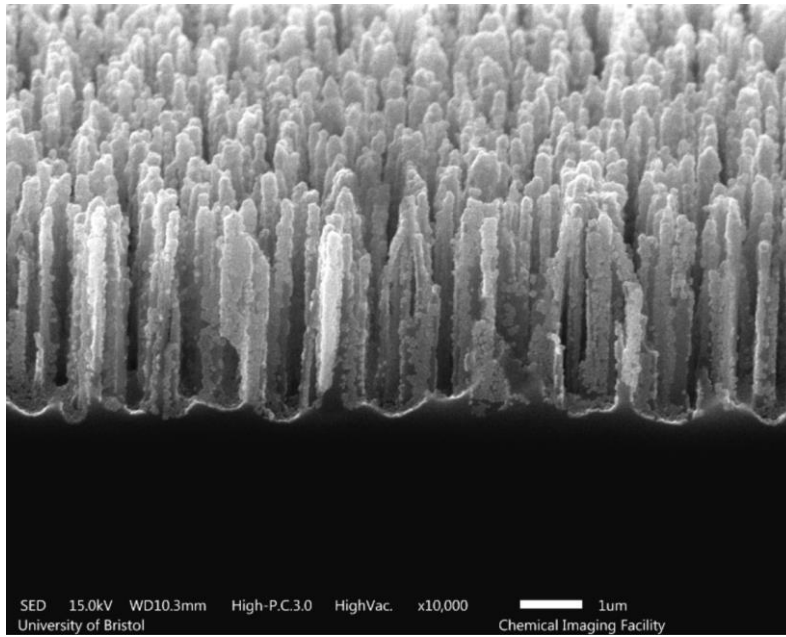


Figure 27. SEM image of black diamond: seeding suspension 3, 20 minute growth.

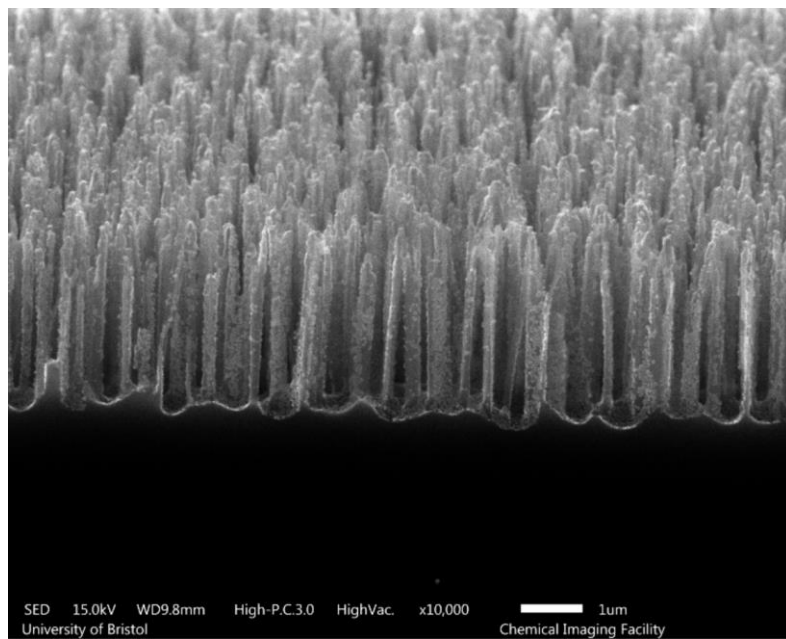
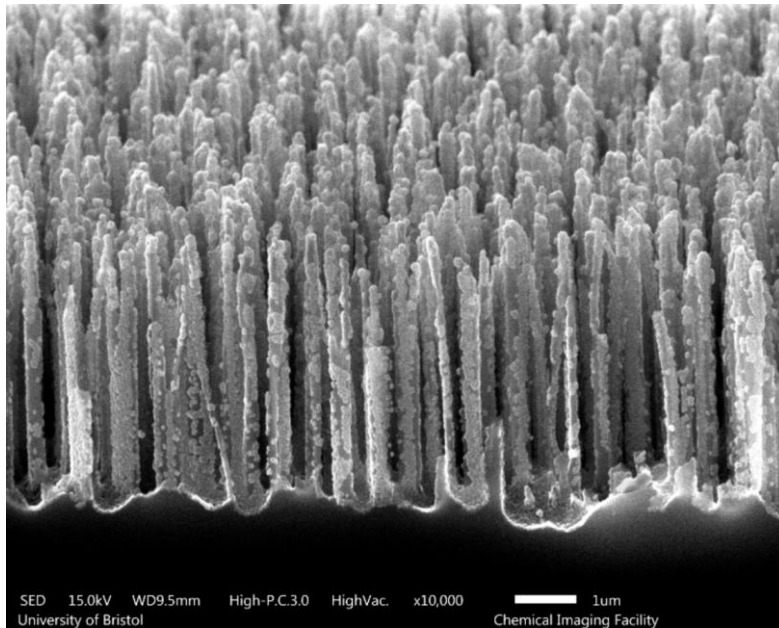


Figure 28. SEM image of black diamond: seeding suspension 4, 15 minute growth.



*Figure 29. SEM image of black diamond: seeding suspension 4, 20 minute growth.*

From these SEM images, it appeared that seeding with suspension 2 produced better quality samples: there seems to be the most consistent coating down the length of the needles on the sample seeded with suspension 2 and grown for 20 minutes.

It was therefore concluded that the additional sonication time of the seeding suspension improved the seeding and therefore the growth due to reducing aggregates of nanodiamonds in suspension and making them more easily dispersed. However, the 20-minute growth still did not seem to give complete coating of the needles so the suspension was sonicated further and longer growth times were trialled.

Suspension 5 was used to seed black silicon samples which were then grown for 25 and 30 minutes and SEM images were taken for analysis.

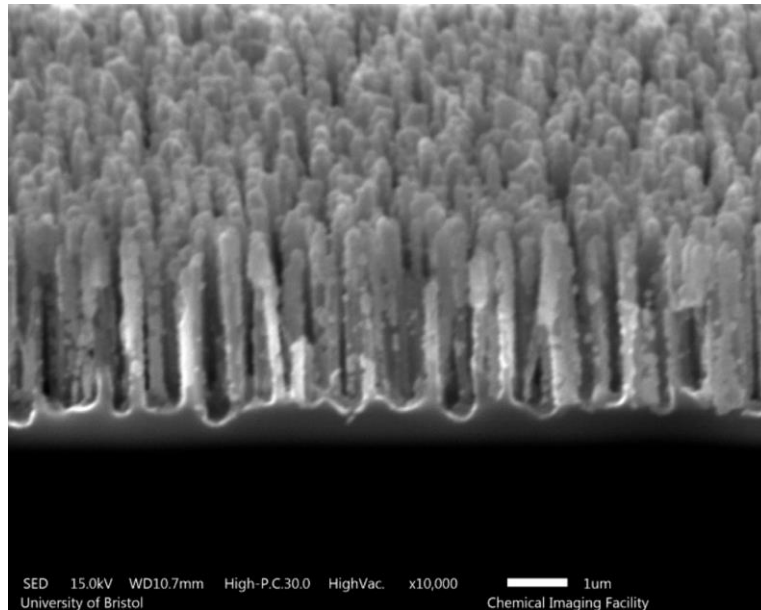


Figure 30. SEM image of black diamond: seeding suspension 5, 25 minute growth.

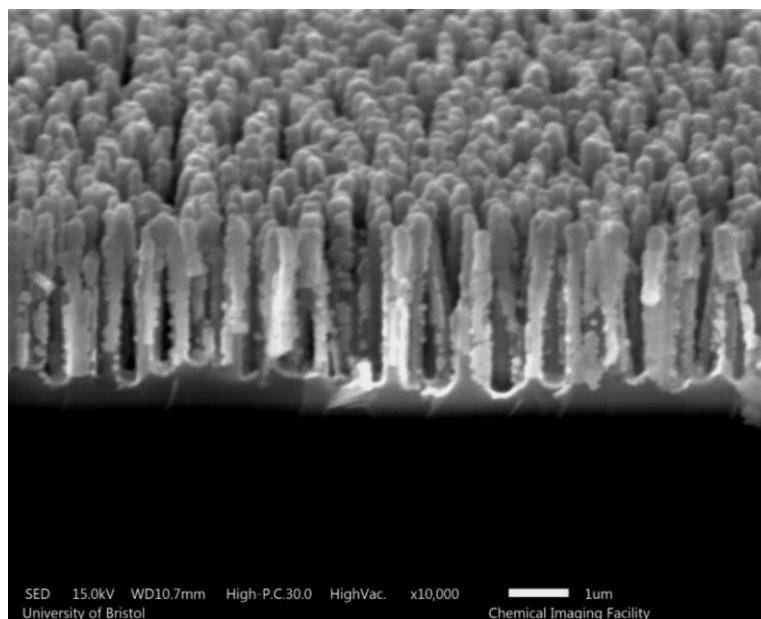
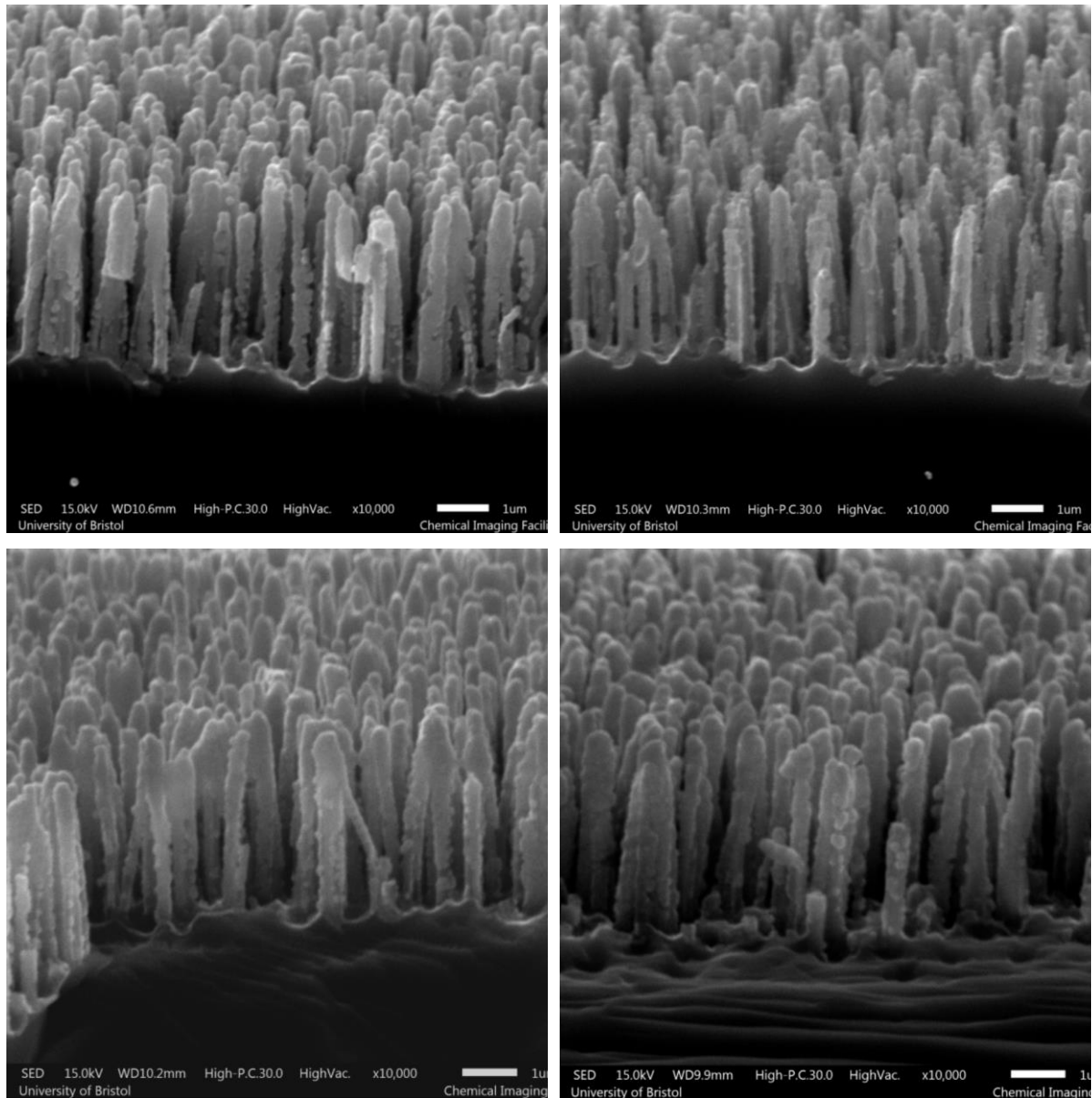


Figure 31. SEM image of black diamond: seeding suspension 5, 30 minute growth.

SEM images showed that the 30-minute growth with suspension 5 appeared to give the best coating while retaining the shape of the needles. Therefore, further black diamond samples were produced in this way to be analysed to check the diamond quality and the consistency of the coating.

Four black silicon samples were seeded with suspension 6 and then grown for 30 minutes, four samples were seeded with suspension 7 and grown for 30 minutes. To check the quality of the diamond and the

consistency of the coating of these samples, SEM and Raman spectra were taken of a random selection of these samples. The SEM images of four different samples are shown in Figure 32.



*Figure 32. SEM images of four black diamond samples, grown for 30 minutes.*

Visually these samples appear very similar, there is good coating of diamond down the length of the needles, but they appear to have retained their original shape and there is little to no clumping together.

Table 3. Needle dimensions of four black diamond samples, grown for 30 minutes. Measurements taken from SEM images.

Sample	Average needle height / $\mu\text{m}$	Average needle width / nm	Needle density / $\mu\text{m}^{-2}$
1	$3.0 \pm 0.4$	$300 \pm 70$	$8 \pm 1.6$
2	$2.6 \pm 0.8$	$300 \pm 50$	$7 \pm 2.3$
3	$3.0 \pm 0.4$	$300 \pm 80$	$8 \pm 2.7$
4	$3.0 \pm 0.5$	$300 \pm 100$	$10 \pm 3.7$

Measurements of the dimensions of the needles from SEM images are shown in Table 3. While there is a fairly high uncertainty associated with these measurements due to the variety of needles within the same sample (10 random needles were measured, including some which appeared to be broken or clumped together), they do indicate that the dimensions of the needles are fairly consistent between these samples.

In previous studies, black diamond with needle lengths ranging from 0.5-20  $\mu\text{m}$  have been tested as antibacterial surfaces. While generally, the nanostructured surfaces were shown to be more effective than flat diamond surfaces, varying the dimensions of the needles affected how effective they were at killing bacteria.<sup>32, 42, 51</sup> A study by Hazell *et al.* tested the bactericidal effect of black diamond needles of different dimensions. The medium needles tested in this study were  $\sim 3.0 \mu\text{m}$  tall, the tip diameter ranged from 300-400 nm and the needle density was  $8 \mu\text{m}^{-2}$ : very similar dimensions to our samples. Death rates of 24-31% of *Escherichia coli* were observed on these needles, suggesting relatively good efficiency for needles of the same dimensions as produced by us.<sup>32</sup> Therefore, it is expected that our samples would be relatively effective against bacteria of a similar type and size. However, it is unclear how they will interact with the bacteria being tested, *Staphylococcus aureus* and *Staphylococcus epidermidis*, which are both Gram-positive and smaller.

## 3.2 Raman

Raman spectroscopy was also performed on several of the final samples to check the diamond quality. A sharp peak at  $1332 \text{ cm}^{-1}$  on Raman spectra arises from crystalline diamond<sup>52</sup>, so it was hoped that this would be observed in the spectra of the coated sample.

The Raman spectrum of black silicon is shown in Figure 33 for comparison: the single large peak at  $939 \text{ cm}^{-1}$  arises from the nanostructured silicon, as this has been reported to occur between 900-1100  $\text{cm}^{-1}$  in the literature.<sup>53</sup> This is different to the typical single-crystal silicon peak at  $520 \text{ cm}^{-1}$  due to the effect the change in structure has on the scattering of light.<sup>54</sup>

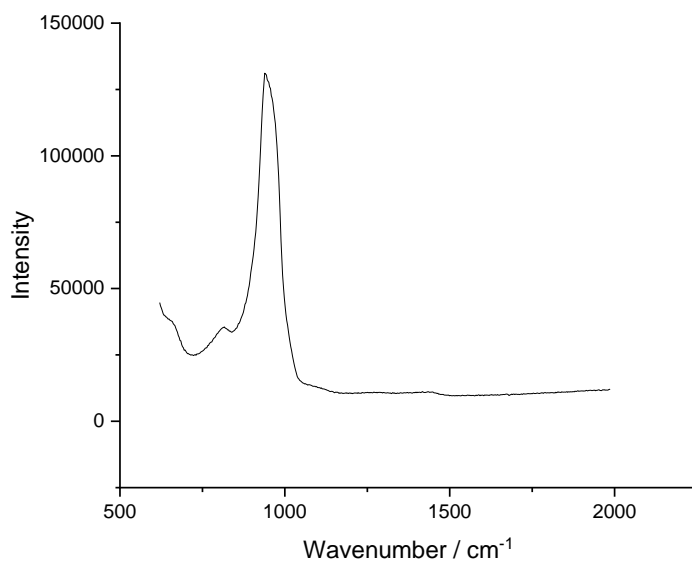


Figure 33. Raman spectrum of black silicon.

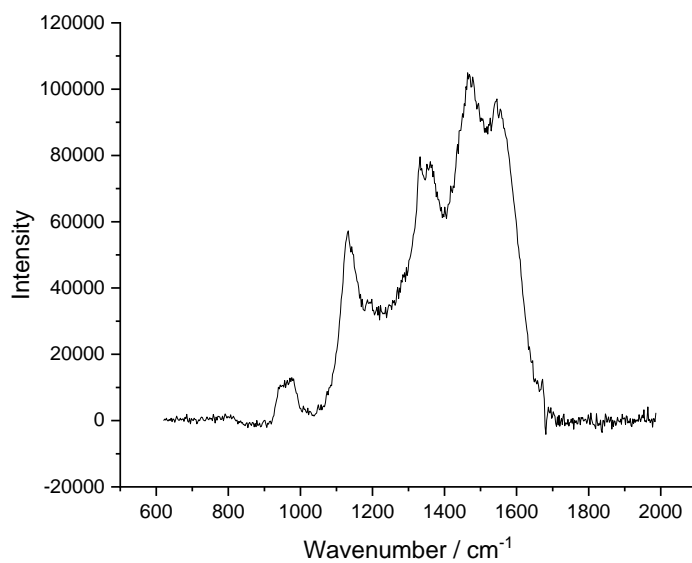


Figure 34. Raman spectrum of black diamond, grown for 30 minutes.

The Raman spectrum of the black diamond sample in Figure 34 shows several significant peaks. Firstly, at a very similar position to the black silicon only sample (959 cm<sup>-1</sup>), there is a relatively low intensity peak from the black silicon. Due to the short growth times of diamond on the black silicon, it would be

expected that a peak from this would show up on the spectrum as there is only a thin transparent diamond layer and also there may not be complete coverage.

There are several other larger peaks which are significant. Firstly, there is a peak at  $1332\text{ cm}^{-1}$  resulting from crystalline diamond having formed on the sample.<sup>52</sup> However, there are several other more intense peaks which give important information on the nature of the diamond formed. Peaks at  $1361\text{ cm}^{-1}$ ,  $1464\text{ cm}^{-1}$ ,  $1546\text{ cm}^{-1}$  are all observed due to the presence of graphite on the sample which is observed on micro and nanocrystalline diamond. The literature shows that a peak arises from the D-band of disordered graphite at approximately  $1355\text{ cm}^{-1}$ , the G-band of amorphous graphite gives a broad peak from  $1500\text{-}1550\text{ cm}^{-1}$  and different  $\text{sp}^2$  clusters can result in a peak around  $1480\text{ cm}^{-1}$ .<sup>52</sup>

Finally, the peak at  $1133\text{ cm}^{-1}$  is a result of *trans*-polyacetylene which has been shown to show up at approximately  $1150\text{ cm}^{-1}$ . This is also often observed in nanocrystalline diamond as *trans*-polyacetylene is formed at the grain boundaries.<sup>55</sup> Due to the nanodiamond seeding and short growth time of this sample, it is expected that the diamond film formed is nanocrystalline.

### 3.3 Fragility experiment

One reason for coating the black silicon with diamond for this application is to make it more robust because black silicon is extremely fragile and the nanoneedles are easily broken.<sup>42</sup> To test this, a simple experiment was designed in which tape was applied to one half of a sample then removed after 10 minutes. Due to the fragility of the black silicon needles, it would be expected that the tape would pull a significant number of them off. The surface of the sample on both sides was compared and checked for damage using SEM. This was tested using black silicon samples and one black diamond sample grown for 20 and 30 minutes.

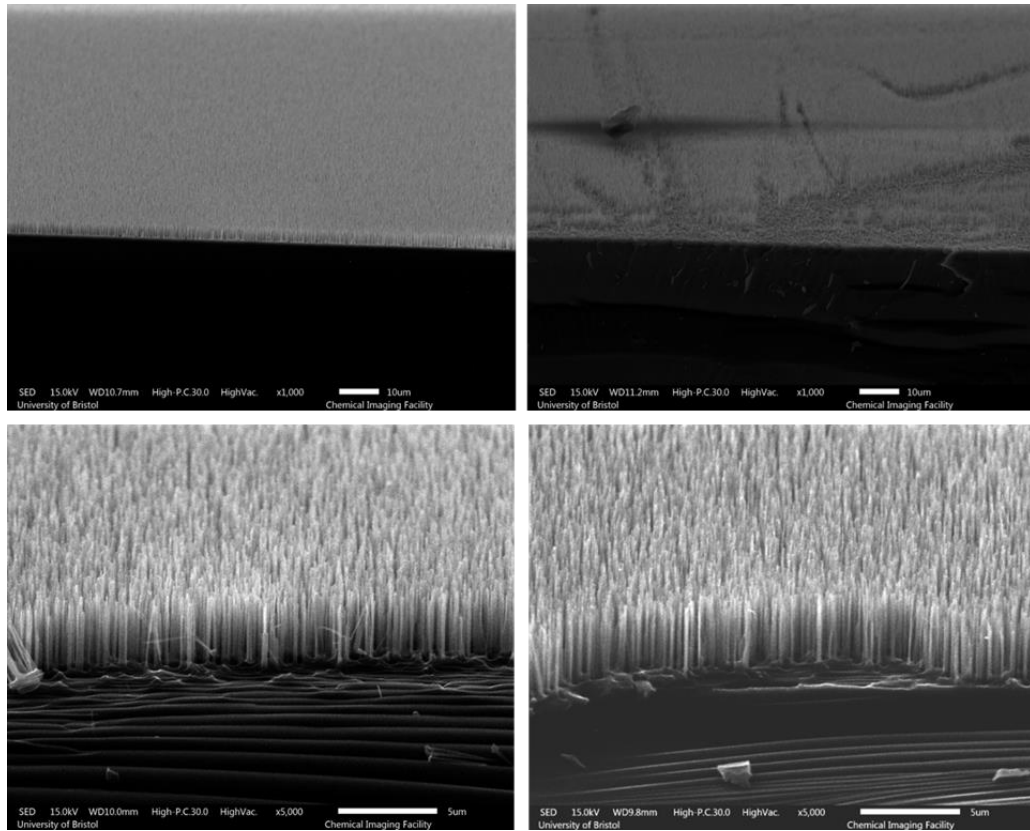
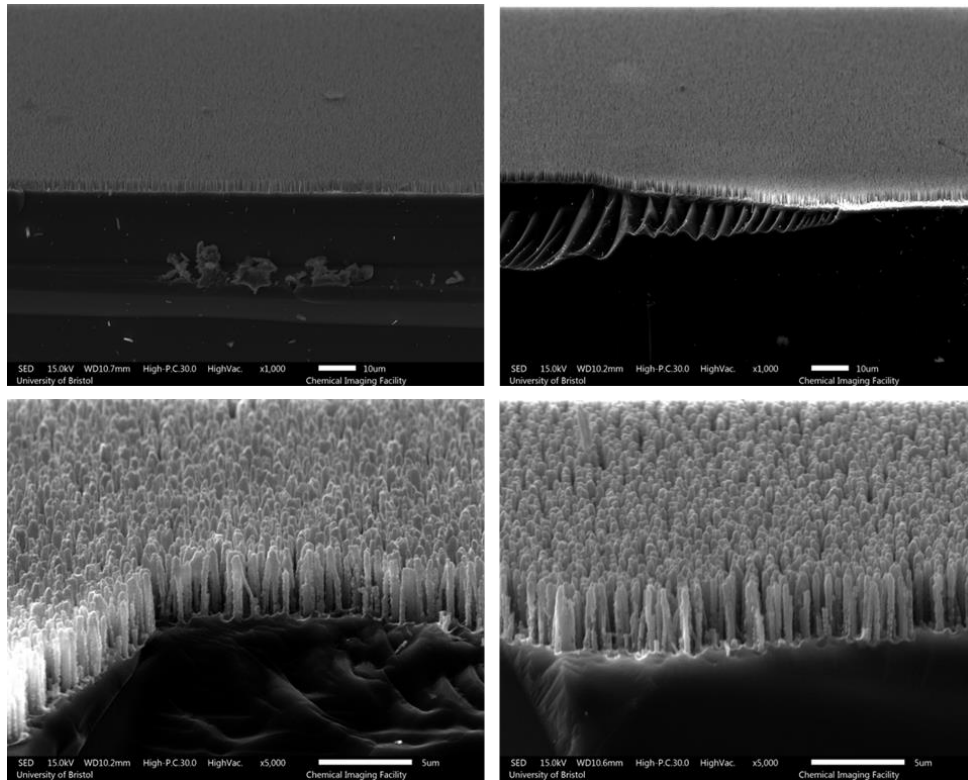


Figure 35. SEM images of untaped (left) and taped (right) black silicon samples.

The top right SEM image where the black silicon sample has been taped appears to show significant areas of the sample where the needles have been damaged compared to the untaped side. However, on the other black silicon sample tested (bottom), no significant differences were observed on the SEM image.



*Figure 36. SEM images of untaped (left) and taped (right) black diamond samples. 20 minute growth (top), 30 minute growth (bottom).*

Both taped and untaped sides of the black diamond sample appear similar, with very little damage on both sides. Compared to the damage to the black silicon by the tape, this could support the claim of increased robustness of the black diamond. However, these results are really not significant due to the extremely small sample size.

## 4 Conclusion

Unfortunately, due to limited time in the lab, the majority of the time was spent optimising the seeding process and growth time to obtain suitable black diamond samples in which the needles were fully coated while the original nanostructure was preserved. Growth times of 30 minutes in the hot filament reactor were found to be optimal and it was observed that increasing the sonication time of the nanodiamond seeding suspension improved the quality of the diamond film grown. Analysis of the dimensions and diamond coating of the samples produced confirm the reproducibility of these samples and comparison with samples used in previous studies suggest that they have the properties to act as effective bactericidal surfaces against Gram-negative bacteria. These samples have since been sent to a biolab in Groningen University in the Netherlands for bactericidal testing using Gram-positive bacteria *Staphylococcus aureus* and *Staphylococcus epidermidis*.

The fragility experiment did not give conclusive results due to the small sample size. This could be adapted and repeated to give better results. However, as black diamond will realistically not be used as an antimicrobial surface in real world applications but instead serves as a good model for examining the interactions between microbes and surface features, testing properties like the toughness is probably not high priority.

## 5 Future Work

Initially, biological testing of the samples using Gram-positive bacteria *Staphylococcus aureus* and *Staphylococcus epidermidis* will be carried out at a biolab in Groningen University in the Netherlands.

Meanwhile, preparation of black diamond samples of the same type will continue in order to produce samples to be used for biological testing using algae. The viability of algae on black diamond surfaces will be investigated for the first time, potentially expanding the applications of this type of surface.

With more time in the lab, it would be useful to fluorine terminate the black diamond samples before biological testing as this has been shown to increase cell death percentages in previous studies. Furthermore, another interesting area to explore is grafting of biological molecules onto amine terminated surfaces to increase their applications. For example, grafting of antibiotic molecules onto bactericidal nanostructured surfaces could massively increase their effectiveness and applications.

Additionally, for future biological testing of bacteria or algae, it would be beneficial to produce a range of samples with variable needle dimensions and spacing to optimise the nanofeatures to the type and size of microorganism being tested.

Finally, while these black diamond surfaces are valuable for testing and modelling the interactions between bacteria and surface features, realistically they will not be used for real world applications due to their fragility. Therefore, in the future, mimicking this type of surface on more standard materials would be beneficial in increasing the real-world applications of this type of surface.

## 6 References

1. S. B. Levy and B. Marshall, *Nature Medicine*, 2004, **10**, S122-S129.
2. A. Penesyanyan, I. T. Paulsen, M. R. Gillings, S. Kjelleberg and M. J. Manefield, *Frontiers in Microbiology*, 2020, **11**.
3. A. S. Lynch and G. T. Robertson, *Annual Review of Medicine*, 2008, **59**, 415-428.
4. M. I. Thoulouze and A. Alcover, *Trends in Microbiology*, 2011, **19**, 257-262.
5. J. F. Briand, *Biofouling*, 2009, **25**, 297-311.
6. P. A. Levin and E. R. Angert, *Cold Spring Harbor Perspectives in Biology*, 2015, **7**, a019216.
7. T. J. Silhavy, D. Kahne and S. Walker, *Cold Spring Harbor Perspectives in Biology*, 2010, **2**, a000414-a000414.
8. J. Louten, in *Essential Human Virology*, Elsevier, 2016, pp. 19-29.
9. J. A. Raven and M. Giordano, *Current Biology*, 2014, **24**, R590-R595.
10. M. P. Schultz, *Biofouling*, 2007, **23**, 331-341.
11. A. Elbourne, R. J. Crawford and E. P. Ivanova, *Journal of Colloid and Interface Science*, 2017, **508**, 603-616.
12. J. Hasan, R. J. Crawford and E. P. Ivanova, *Trends in Biotechnology*, 2013, **31**, 295-304.
13. A. Penesyanyan, M. Gillings and I. T. Paulsen, *Molecules*, 2015, **20**, 5286-5298.
14. J. C. Tiller, C. J. Liao, K. Lewis and A. M. Klibanov, *Proceedings of the National Academy of Sciences of the United States of America*, 2001, **98**, 5981-5985.
15. E. P. Ivanova, J. Hasan, V. K. Truong, J. Y. Wang, M. Raveggi, C. Fluke and R. J. Crawford, *Applied Microbiology and Biotechnology*, 2011, **91**, 1149-1157.
16. H. Murata, R. R. Koepsel, K. Matyjaszewski and A. J. Russell, *Biomaterials*, 2007, **28**, 4870-4879.
17. A. C. Pinho and A. P. Piedade, *Polymers*, 2020, **12**.
18. E. P. Ivanova, J. Hasan, H. K. Webb, V. K. Truong, G. S. Watson, J. A. Watson, V. A. Baulin, S. Pogodin, J. Y. Wang, M. J. Tobin, C. Lobbe and R. J. Crawford, *Small*, 2012, **8**, 2489-2494.
19. J. Hasan, H. K. Webb, V. K. Truong, G. S. Watson, J. A. Watson, M. J. Tobin, G. Gervinskas, S. Juodkazis, J. Y. Wang, R. J. Crawford and E. P. Ivanova, *Langmuir*, 2012, **28**, 17404-17409.
20. D. E. Mainwaring, S. H. Nguyen, H. Webb, T. Jakubov, M. Tobin, R. N. Lamb, A. H. F. Wu, R. Marchant, R. J. Crawford and E. P. Ivanova, *Nanoscale*, 2016, **8**, 6527-6534.
21. A. Solga, Z. Cerman, B. F. Striffler, M. Spaeth and W. Barthlott, *Bioinspiration & Biomimetics*, 2007, **2**, S126-S134.
22. Y. H. Liu and G. J. Li, *Journal of Colloid and Interface Science*, 2012, **388**, 235-242.

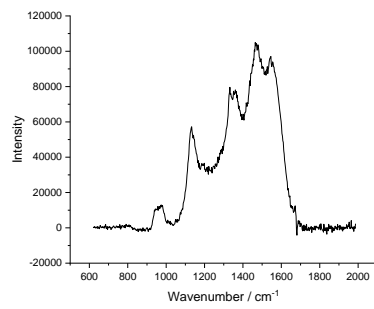
23. G. S. Watson, D. W. Green, L. Schwarzkopf, X. Li, B. W. Cribb, S. Myhra and J. A. Watson, *Acta Biomaterialia*, 2015, **21**, 109-122.
24. C. D. Bandara, S. Singh, I. O. Afara, A. Wolff, T. Tesfamichael, K. Ostrikov and A. Oloyede, *Acs Applied Materials & Interfaces*, 2017, **9**, 6746-6760.
25. S. M. Kelleher, O. Habimana, J. Lawler, B. O' Reilly, S. Daniels, E. Casey and A. Cowley, *ACS Applied Materials & Interfaces*, 2016, **8**, 14966-14974.
26. R. J. Jiang, L. W. Hao, L. J. Song, L. M. Tian, Y. Fan, J. Zhao, C. Z. Liu, W. H. Ming and L. Q. Ren, *Chemical Engineering Journal*, 2020, **398**.
27. Pixabay, <https://pixabay.com/photos/lotus-leaf-water-drop-lotus-water-2420205/>, (accessed 22/02/2022).
28. S. Pogodin, J. Hasan, V. A. Baulin, H. K. Webb, V. K. Truong, T. H. P. Nguyen, V. Boshkovikj, C. J. Fluke, G. S. Watson, J. A. Watson, R. J. Crawford and E. P. Ivanova, *Biophysical Journal*, 2013, **104**, 835-840.
29. J. Hasan, H. K. Webb, V. K. Truong, S. Pogodin, V. A. Baulin, G. S. Watson, J. A. Watson, R. J. Crawford and E. P. Ivanova, *Applied Microbiology and Biotechnology*, 2013, **97**, 9257-9262.
30. F. Xue, J. Liu, L. Guo, L. Zhang and Q. Li, *Journal of Theoretical Biology*, 2015, **385**, 1-7.
31. A. Velic, J. Hasan, Z. Y. Li and P. Yarlagadda, *Biophysical Journal*, 2021, **120**, 217-231.
32. G. Hazell, P. W. May, P. Taylor, A. H. Nobbs, C. C. Welch and B. Su, *Biomaterials Science*, 2018, **6**, 1424-1432.
33. J. Jenkins, J. Mantell, C. Neal, A. Gholinia, P. Verkade, A. H. Nobbs and B. Su, *Nature Communications*, 2020, **11**.
34. J. Jenkins, M. I. Ishak, M. Eales, A. Gholinia, S. Kulkarni, T. F. Keller, P. W. May, A. H. Nobbs and B. Su, *iScience*, 2021, **24**, 102818.
35. C. M. Bhadra, V. Khanh Truong, V. T. H. Pham, M. Al Kobaisi, G. Seniutinas, J. Y. Wang, S. Juodkazis, R. J. Crawford and E. P. Ivanova, *Scientific Reports*, 2015, **5**, 16817.
36. S. Wu, F. Zuber, J. Brugger, K. Maniura-Weber and Q. Ren, *Nanoscale*, 2016, **8**, 2620-2625.
37. M. N. Dickson, E. I. Liang, L. A. Rodriguez, N. Vollereaux and A. F. Yee, *Biointerphases*, 2015, **10**.
38. L. E. Fisher, Y. Yang, M.-F. Yuen, W. Zhang, A. H. Nobbs and B. Su, *Biointerphases*, 2016, **11**, 011014.
39. E. P. Ivanova, J. Hasan, H. K. Webb, G. Gervinskas, S. Juodkazis, V. K. Truong, A. H. F. Wu, R. N. Lamb, V. A. Baulin, G. S. Watson, J. A. Watson, D. E. Mainwaring and R. J. Crawford, *Nature Communications*, 2013, **4**.
40. J. Hasan, Y. A. Xu, T. Yarlagadda, M. Schuetz, K. Spann and P. Yarlagadda, *Acs Biomaterials Science & Engineering*, 2020, **6**, 3608-3618.

41. C.-H. Hsu, J.-R. Wu, Y.-T. Lu, D. J. Flood, A. R. Barron and L.-C. Chen, *Materials Science in Semiconductor Processing*, 2014, **25**, 2-17.
42. O. Dunseath, E. J. W. Smith, T. Al-Jeda, J. A. Smith, S. King, P. W. May, A. H. Nobbs, G. Hazell, C. C. Welch and B. Su, *Scientific Reports*, 2019, **9**.
43. M. C. Salvadori, W. W. R. Araújo, F. S. Teixeira, M. Cattani, A. Pasquarelli, E. M. Oks and I. G. Brown, *Diamond and Related Materials*, 2010, **19**, 324-328.
44. M. N. R. Ashfold, P. W. May, C. A. Rego and N. M. Everitt, *Chemical Society Reviews*, 1994, **23**, 21.
45. P. W. May, *Philosophical Transactions of the Royal Society of London Series a-Mathematical Physical and Engineering Sciences*, 2000, **358**, 473-495.
46. J. J. Gracio, Q. H. Fan and J. C. Madaleno, *Journal of Physics D-Applied Physics*, 2010, **43**.
47. J. Raymakers, K. Haenen and W. Maes, *Journal of Materials Chemistry C*, 2019, **7**, 10134-10165.
48. D. Zhu, J. A. Bandy, S. Li and R. J. Hamers, *Surface Science*, 2016, **650**, 295-301.
49. S. Szunerits, C. E. Nebel and R. J. Hamers, *MRS Bulletin*, 2014, **39**, 517-524.
50. J. McGrath, MSc, University of Bristol, 2020.
51. P. W. May, M. Clegg, T. A. Silva, H. Zanin, O. Fatibello, V. Celorrio, D. J. Fermin, C. C. Welch, G. Hazell, L. Fisher, A. Nobbs and B. Su, *Journal of Materials Chemistry B*, 2016, **4**, 5737-5746.
52. R. Haubner and M. Rudigier, *Nineteenth European Conference on Chemical Vapor Deposition (Eurocvd 19)*, 2013, **46**, 71-78.
53. I. Iatsunskiy, S. Jurga, V. Smyntyna, M. Pavlenko, V. Myndrul and A. Zaleska, Brussels, BELGIUM, 2014.
54. S. Jurecka, E. Pincik, K. Imamura, T. Matsumoto and H. Kobayashi, *Journal of Electrical Engineering-Elektrotechnicky Casopis*, 2019, **70**, 58-64.
55. R. Pfeiffer, H. Kuzmany, P. Knoll, S. Bokova, N. Salk and B. Gunther, *Diamond and Related Materials*, 2003, **12**, 268-271.

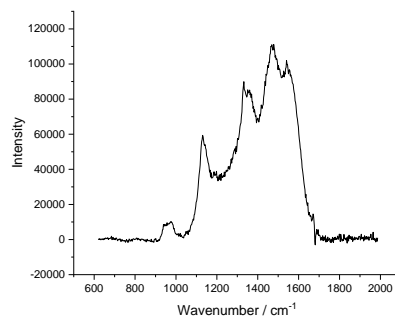
## 7 Appendix

### 7.1 Raman

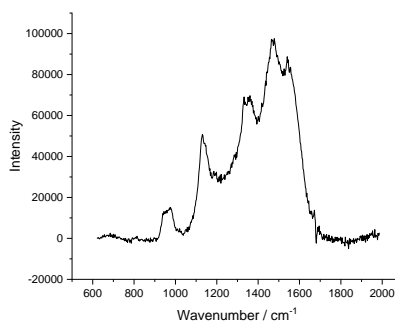
Additional Raman spectra were taken of different areas of several of the 30 minute growth samples to be sent for biological testing.



(a)

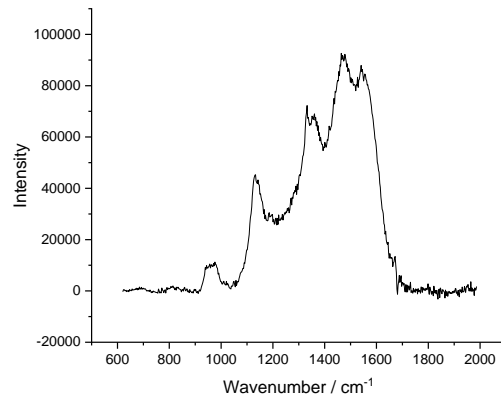


(b)

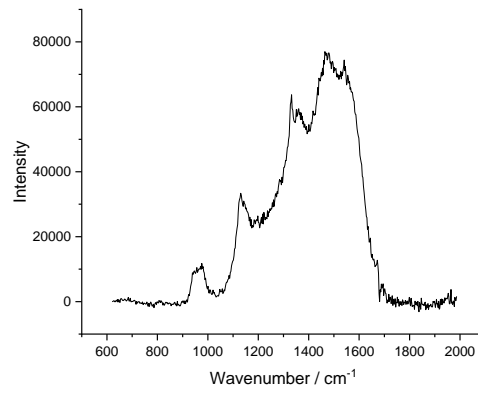


(c)

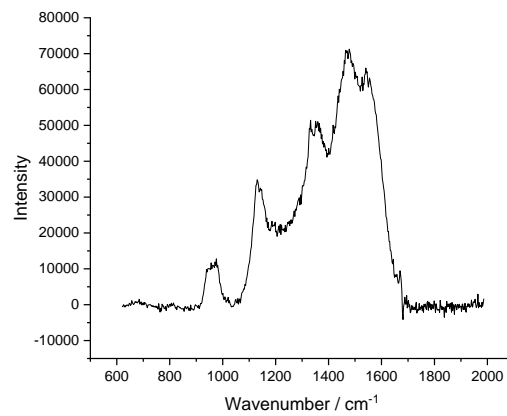
Figure 37. Raman spectra of 30 minute growth black diamond using 514 nm wavelength. Spectra a, b and c are for three different areas of the same sample.



(a)

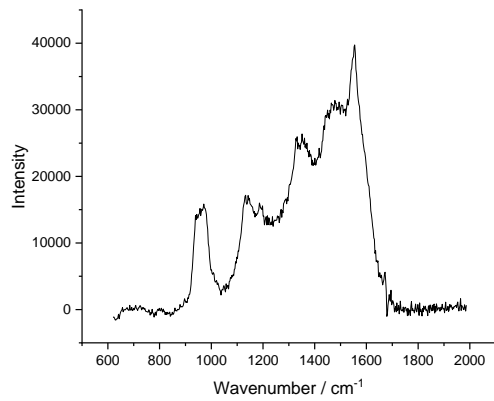


(b)

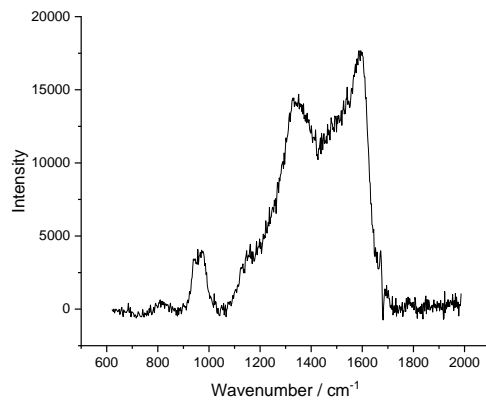


(c)

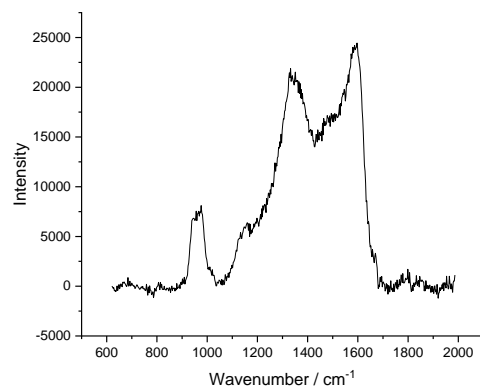
Figure 38. Raman spectra of 30 minute growth black diamond using 514 nm wavelength. Spectra a, b and c are for three different areas of the same sample.



(a)



(b)



(c)

Figure 39. Raman spectra of 30 minute growth black diamond using 514 nm wavelength. Spectra a, b and c are for three different areas of the same sample.